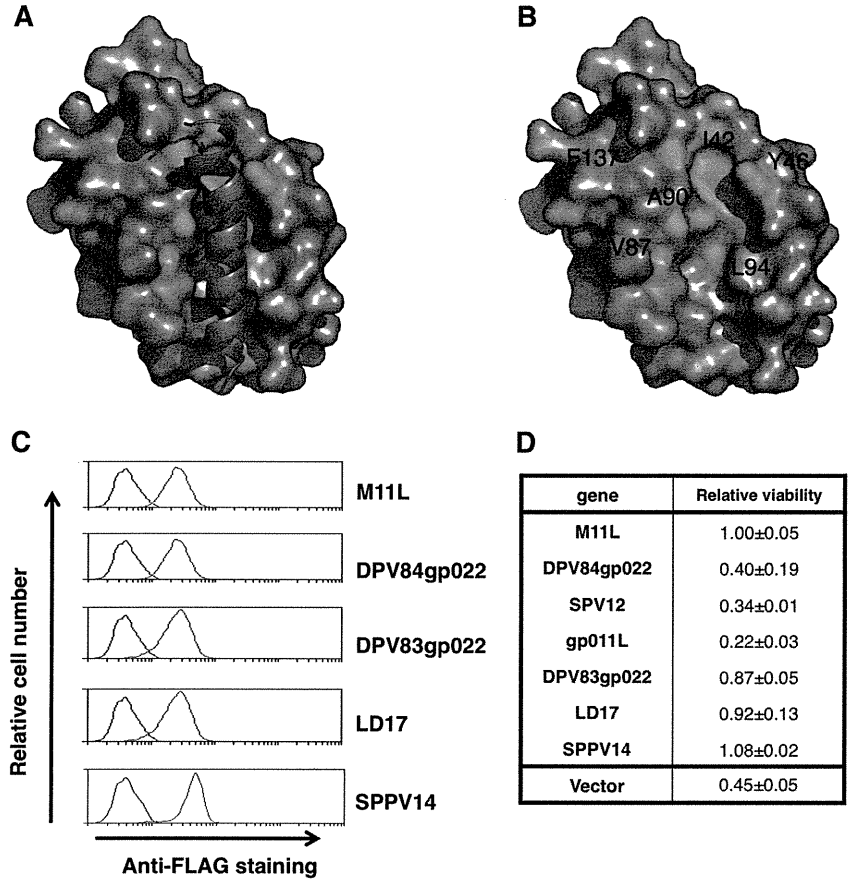

gene	Relative viability
M11L	1.00±0.05
DPV84gp022	0.40±0.19
SPV12	0.34±0.01
gp011L	0.22±0.03
DPV83gp022	0.87±0.05
LD17	0.92±0.13
SPPV14	1.08±0.02
Vector	0.45±0.05

FIG 2 Some putative vBcl-2 proteins block apoptosis. (A) Cartoon of the binding interface formed by the M11L-Bak complex (40). The M11L surface is shown in gray, and residues conserved between SPPV14 and M11L (Fig. 1B) that form part of the canonical binding groove in M11L are shaded in cyan. The Bak BH3 peptide is shown in orange. (B) Cartoon of the binding interface formed by the M11L-Bak complex. The colors are as in panel A, and the Bak BH3 peptide is removed for clarity. (C) The expression of FLAG-tagged viral proteins in MEFs was detected by flow cytometry. MEFs expressing novel vBcl-2 proteins were fixed and stained with an anti-FLAG antibody (red lines). The staining of MEFs expressing the empty vector is shown as the negative control (black lines). (D) The viability of MEFs expressing the empty vector, M11L, or poxvirus vBcl-2 proteins treated with etoposide (2.5 μM) for 24 h was determined by propidium iodide (PI) exclusion. The relative viability was determined by normalizing to that of M11L-expressing cells treated with etoposide. The data represent means ± standard deviations (SD) of two experiments performed with each cell line.

encoding BH3-only proteins were transiently transfected into Phoenix Ecotropic packaging cells, and viral supernatants were used to infect cells as described previously (9). Cell viability in both short-term assays and long-term assays of colony formation was determined as described previously (9). Long-term survival is expressed as a percentage of the number of colonies obtained relative to the number of colonies obtained after retroviral infection with empty parental retrovirus.

Bak activation was assessed by infecting 1×10^6 Jurkat cells, Jurkat cells expressing Bcl-2, or Bak- and Bax-deficient Jurkat cells at a multiplicity of infection (MOI) of 10 with VVEGFP (control wild-type vaccinia virus), VVΔF1L (F1L-deficient virus), or VVΔF1L-FLAG-SPPV14 (F1L-deficient virus expressing FLAG-tagged SPPV14). Six hours postinfection, the cells were fixed in 0.25% paraformaldehyde, permeabilized with 500 μg/ml (0.05%) digitonin (Sigma-Aldrich), and stained with a conformation-specific anti-Bak Ab-1 antibody (Oncogene Research Products) (28). Phycoerythrin-conjugated anti-mouse antibody was used to counterstain the cells (Jackson ImmunoResearch) before analysis by flow cytometry (FACScan; Becton Dickinson) using the FL-2 channel equipped with a 585-nm filter (42-nm band-pass). Data were analyzed using CellQuest software.

Protein production. The cDNA of SPPV14 was used to amplify the region coding for residues 1 to 145 of SPPV14 (deleting the C-terminal 31 amino acids, referred to as SPPV14ΔC31), which was cloned into the pET DUET vector (Invitrogen) using an introduced 5′ BamHI restriction site and 3′ EcoRI site, followed by a stop codon, and expressed in *Escherichia coli* BL21(DE3) pLysS cells. After homogenization in lysis buffer (20 mM Tris-HCl, pH 8.0, 150 mM NaCl, 10 mM 2-mercaptoethanol), the cell lysate was centrifuged and filtered prior to loading onto a 1-ml His-Trap column (Amersham). The protein was eluted in lysis buffer supplemented with 250 mM imidazole and subjected to gel filtration chromatography in 20 mM HEPES, pH 7.5, 150 mM NaCl, and 10 mM dithiothreitol (DTT) using a Superdex 200 column (Amersham), where it eluted as a single peak.

Immunoprecipitation and immunoblotting. The transfection and metabolic labeling of the human embryonic kidney (HEK293T cells with [^{35}S]methionine/[^{35}S]cysteine (NEN) have been described previously (33, 46). Immunoprecipitation of SPPV14 with Bak or Bax was performed using mouse monoclonal anti-FLAG (M2; Sigma) or anti-HA (HA11; Covance) antibody in buffer containing 20 mM Tris-HCl, pH 7.4, 135 mM NaCl, 1% Triton X-100, 10% glycerol in the presence of protease inhibitor (Roche). Control immunoprecipitations were performed using an anti-mouse Glu-Glu (MMS-115R; CRP) antibody. Proteins were resolved by SDS-PAGE (Novex gels; Invitrogen), transferred onto nitrocellulose membranes, and detected with X-ray film (Hyperfilm; GE Healthcare).

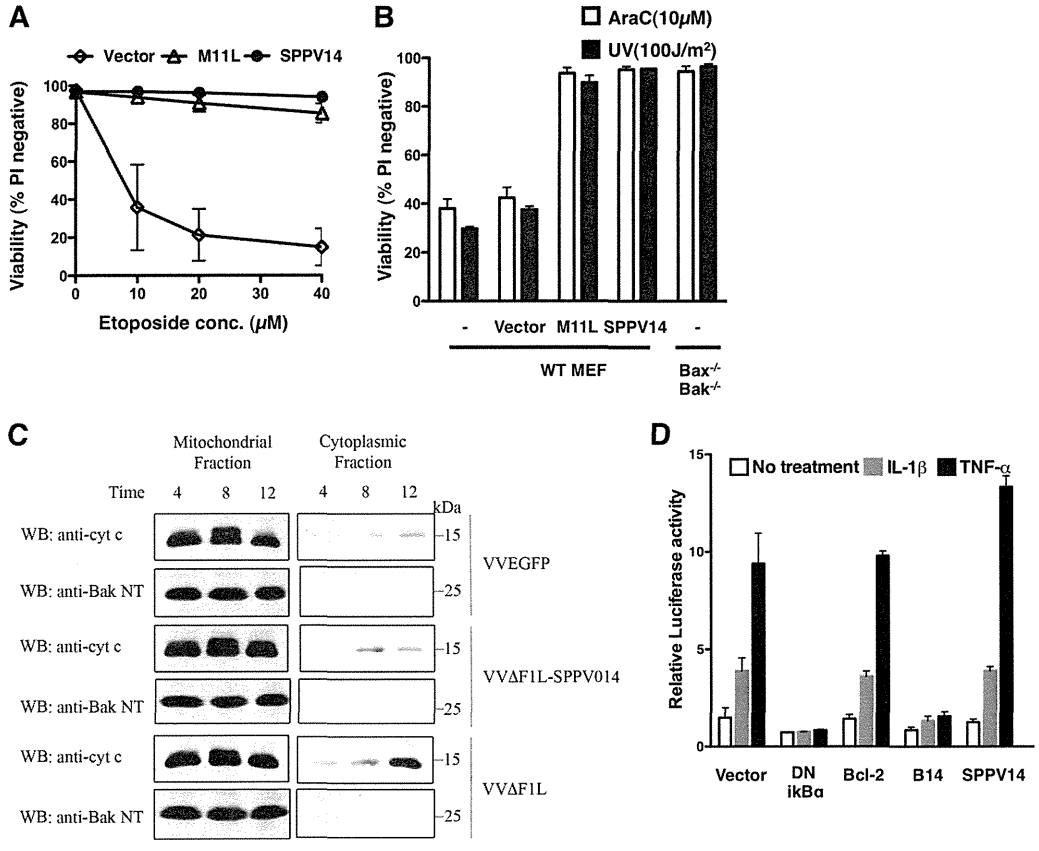

FIG 3 SPPV14 inhibits apoptosis, but not NF-κB activation. (A) Sheeppox virus SPPV14 is functionally comparable to myxoma virus M11L. Shown is the viability of wild-type (WT) MEFs expressing M11L or SPPV14, or the vector control, 24 h after treatment with 0 to 40 μM etoposide. (B) SPPV14 blocks apoptosis induced by diverse agents. Shown is the viability of MEFs (described in the legend to Fig. 1B) 24 h after treatment with 10 μM AraC or exposure to UV irradiation (100 J/m^2). The bars on the right show the viability of similarly treated Bax/Bak-doubly deficient MEFs. (C) SPPV14 prevents cytochrome *c* release. Jurkat cells were infected with VVEGFP, VVΔF1L-SPPV014, and VVΔF1L at an MOI of 10 for 4, 8, and 12 h. Mitochondrial pellets and cytoplasmic supernatants were separated via ultracentrifugation after treatment with digitonin. The mitochondrial pellets were resuspended in lysis buffer containing 0.1% Triton X-100, and 20% of the mitochondrial fractions and 50% of the cytoplasmic fractions were subjected to SDS-PAGE and immunoblotted with anti-cytochrome *c* and anti-Bak NT antibody as a control. WB, Western blotting. (D) SPPV14 does not block NF-κB activation induced by IL-1β or TNF-α. HEK293 cells were transiently transfected with an NF-κB luciferase reporter plasmid and the empty vector, dominant-negative (DN) IκBα, Bcl-2, B14, or SPPV14. The relative luciferase activity was measured 8 h after treatment with IL-1β (100 ng/ml) or TNF-α (100 ng/ml). The data represent means ± SD from 2 independent experiments.

Vaccinia virus production. SPPV14 cDNA was subcloned into pSC66, which places the gene under the control of a poxvirus promoter to generate VVΔF1L-FLAG-SPPV14 (17). Recombinant VVΔF1L-FLAG-SPPV14 was generated by homologous recombination of pSC66-FLAG-SPPV14 into the thymidine kinase locus of VVΔF1L, as described previously (17). In brief, 1 × 10^6 baby green monkey kidney (BGMK) cells were transfected with 5 μg of pSC66-Flag-SPPV14 and infected with VVΔF1L at an MOI of 0.05. Recombinant viruses were selected by growth on HuTK$^-$-143B cells in the presence of 5-bromodeoxyuridine (Sigma-Aldrich) and plaque purification using 5-bromo-4-chloro-3-indolyl-β-D-galactopyranoside (Rose Scientific Ltd.) to visualize β-galactosidase-positive viruses. All viruses were grown on BGMK cells.

Cytochrome *c* release. Jurkat cells (1 × 10^6) were infected with VVEGFP, VVΔF1L-SPPV014, and VVΔF1L at an MOI of 5 at 4, 8, and 12 h of infection. The cells were permeabilized in lysis buffer containing 75 mM NaCl, 1 mM NaH_2PO_4, 8 mM Na_2HPO_4, 250 mM sucrose, and 190 μg/ml of digitonin (Sigma-Aldrich), and the lysates were incubated on ice for 10 min (62). Mitochondrial and cytoplasmic fractions were separated by ultracentrifugation at 10,000 × *g* for 5 min. The mitochondrial pellet was resuspended in Triton X-100 lysis buffer containing 25 mM Tris, pH 8.0, and 0.1% Triton X-100 (Fisher Scientific). Samples were subjected to SDS-PAGE and immunoblotted with mouse anti-cytochrome *c* (BD PharMingen) and anti-Bak NT as a control.

PARP cleavage assay. To detect cleavage of poly-ADP ribose polymerase (PARP), Jurkat cells (1 × 10^6) were mock infected or infected with VVEGFP, VVΔF1L-SPPV014, and VVΔF1L at an MOI of 5. Cells were harvested 4, 8, 12, and 16 h postinfection and lysed in SDS-PAGE sample buffer containing 8 M urea. Samples were subjected to SDS-PAGE and immunoblotted with anti-PARP (BD PharMingen), anti-β-tubulin (EMC Bioscience), and anti-I3L to detect virus infection.

Solution competition assays. Solution competition assays using the Biacore optical biosensor were performed as described previously (9), using identical BH3 domain peptides and 10 nM SPPV14ΔC31.

Yeast colony assays. *Saccharomyces cerevisiae* W303α cells were cotransformed with pGALL(TRP) vector only, pGALL(TRP)-Bcl-x_L, or pGALL(TRP)-DPV022 and pGALL(Leu)-Bak or pGALL(Leu)-Bax. pGALL(TRP) and pGALL(Leu) place genes under the control of a galactose-inducible promoter (29). Cells were spotted as 5-fold serial dilutions onto medium containing 2% (wt/vol) galactose (inducing [ON]), which induces protein expression, or 2% (wt/vol) glucose (repressing [OFF]), which prevents protein expression, as previously described (37). Plates were incubated for 48 h at 30°C and then photographed.

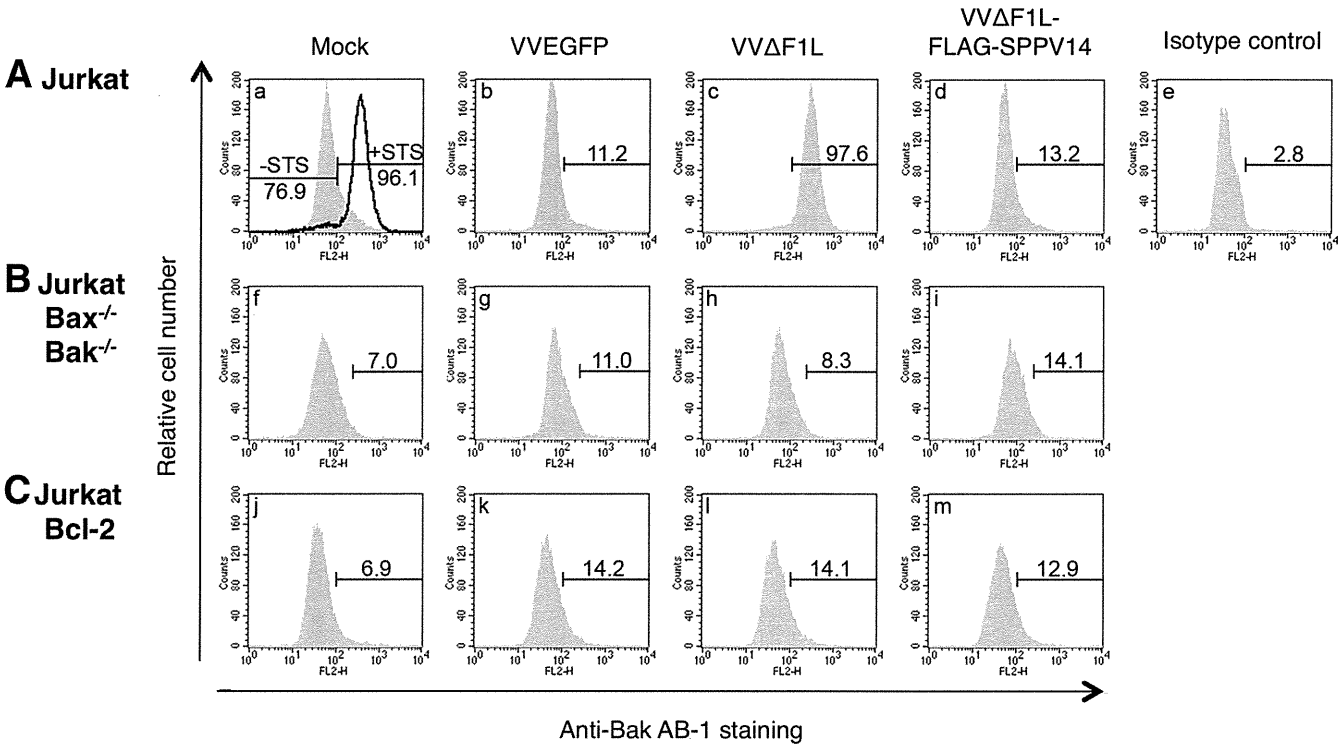

FIG 4 SPPV14 can functionally replace F1L during vaccinia virus infection. (A to C) SPPV14 inhibits Bak activation during vaccinia virus infection. Wild-type (A), Bax/Bak-doubly deficient (B), or Bcl-2-overexpressing (C) Jurkat cells were mock infected or infected with VVEGFP, VVΔF1L, or VVΔF1L-FLAG-SPPV14 (F1L-deficient virus expressing FLAG-tagged SPPV14) vaccinia virus. Bak activation was detected 6 h later by flow cytometric analyses of cells stained with the conformation-specific anti-Bak Ab-1 antibody (28). Positive-control mock-infected cells were treated with the broad-spectrum kinase inhibitor staurosporine (+STS) (A, a), known to induce apoptosis in many cell types. The bars mark the populations that contained activated Bak. Experiments were performed in triplicate. Fractions of Bak-activated cells are given as percentages.

RESULTS

Identifying putative viral Bcl-2 homologs. Although proteins such as Epstein-Barr virus BHRF1 (30) and adenovirus E1B19K (66) were first isolated due to their roles in modulating host-pathogen interactions during infection and in extending the life span of infected cells, they were later recognized as viral homologs of Bcl-2 (vBcl-2) by virtue of their sequence similarity to mammalian Bcl-2 (11). In contrast, herpesvirus saimiri-encoded ORF16 (54) and fowlpox virus-encoded FPV039 (1) were specifically recognized due to sequence similarity to mammalian Bcl-2. Aside from these readily identifiable viral Bcl-2-related proteins, the recent molecular and structural characterization of proteins such as M11L in myxoma virus (40, 59) and F1L in vaccinia virus (21, 42, 63), which appear to be unrelated to Bcl-2 by conventional sequence comparisons, has opened up another approach to identifying vBcl-2 proteins.

By searching for putative proteins that are related by sequence to M11L instead of mammalian Bcl-2, we circumvented the need for conventional genetic or functional screens in order to identify putative antiapoptotic factors encoded by other organisms. In a BLASTP search of the NCBI database (40), the top hits included six sequences that encode putative open reading frames (ORFs) from deerpox virus (DPV83gp022 and DPV84gp022), swinepox virus (SPV12), shope fibroma virus (gp011L), lumpy skin disease virus (LD17), and sheeppox virus (SPPV14) (Fig. 1A). Even though the overall sequence similarity to M11L was low, the critical residues forming the canonical binding groove in M11L (40) were conserved in all six proteins, strongly suggesting the presence of an analogous BH3 binding grove in these proteins (Fig. 1B and 2A and B).

To test if these ORFs encode antiapoptotic proteins, we expressed tagged versions of all six proteins in MEFs (Fig. 2C) and assessed their abilities to counter killing induced by the cytotoxic drug etoposide (Fig. 2D). DPV83gp022, LD17, and SPPV14 potently inhibited etoposide-induced killing, whereas DPV84gp022, swinepox virus (SPV12), and shope fibroma virus (gp011L) did not afford protection against etoposide, even though they were abundantly expressed. Interestingly, we noted that four residues (M52, T67, L68, and A71) in the binding groove of M11L are likely to be important for function, since the identified DPV84gp022, SPV12, and shope (rabbit) fibroma virus gp011L, which do not protect against apoptosis, have critical substitutions for these residues (see Fig. S1 in the supplemental material), possibly pointing to a biological function that does not involve apoptosis. We elected to focus further studies on SPPV14, since it was the most potent (Fig. 2D) out of all 6 identified putative vBcl-2 proteins and afforded protection against etoposide that appeared superior to that of M11L. Notably, SPPV14 shows 22% sequence identity to M11L. However, significantly higher conservation was apparent in the region corresponding to the central α5 helix that constitutes the BH1 region in M11L (10/21 amino acids; ~50%) (Fig. 1B).

Sheeppox virus SPPV14 is a potent inhibitor of mitochondrially mediated cell death. To extend the functional analysis, we examined the dose response following etoposide treatment.

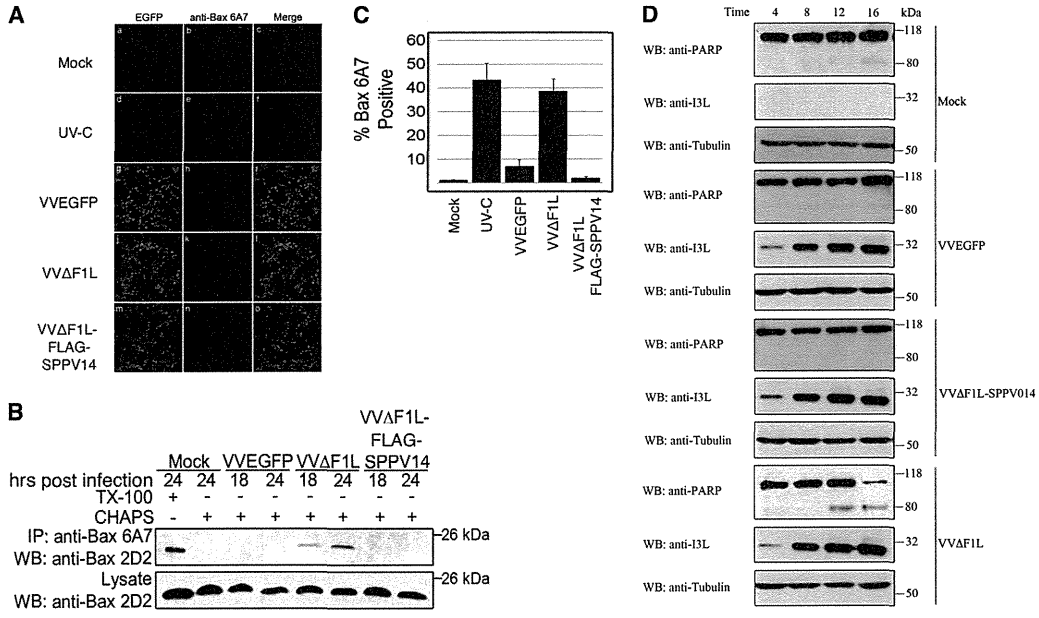

FIG 5 SPPV14 inhibits Bax activation during vaccinia virus infection. (A) HeLa cells were infected with VVEGFP, VVΔF1L, or VVΔF1L-FLAG-SPPV14 and incubated for 24 h. Infected cells or UV-C-irradiated HeLa cells were fixed and stained with the conformation-specific anti-Bax antibody 6A7, which specifically recognizes activated Bax (14, 31). (B) HeLa cells infected with VVEGFP, VVΔF1L, or VVΔF1L-FLAG-SPPV14 were lysed with Triton X-100 or CHAPS {3-[(3-cholamidopropyl)-dimethylammonio]-1-propanesulfonate}-based buffers and immunoprecipitated (IP) using the conformation-specific anti-Bax antibody 6A7. The immunoprecipitants were subjected to SDS-PAGE and blotted with the anti-Bax antibody 2D2, an antibody that recognizes all forms of Bax in immunoblots. (C) SPPV14 inhibits Bax activation induced by VVΔF1L. HeLa cells infected with VVEGFP, VVΔF1L, or VVΔF1L-FLAG-SPPV14 were incubated for 24 h and fixed, and Bax activation was measured by staining with anti-Bax 6A7 antibody (31) that specifically recognizes activated Bax. The data were quantified by counting 200 cells per experiment; means and SD of three replicate experiments are shown. UV-C, positive-control UV-irradiated HeLa cells. (D) SPPV14 inhibits PARP cleavage induced by VVΔF1L. Jurkat cells were mock infected or infected with VVEGFP, VVΔF1L-SPPV14, or VVΔF1L at an MOI of 5. Samples were collected 4, 8, 12, and 16 h postinfection, and the cells were lysed in SDS-PAGE sample buffer containing 8 M urea. Samples were subjected to SDS-PAGE and immunoblotted for PARP to determine the trigger of apoptosis; β-tubulin was used as a loading control and I3L as a sign of infection.

SPPV14 proved to be as efficacious as M11L (Fig. 3A), and its ability to counter killing induced by other agents, such as AraC or UV irradiation, was also comparable (Fig. 3B). Furthermore, SPPV14 appears to act at the mitochondrial checkpoint and not at the level of caspases, since it potently inhibits cytochrome *c* release (Fig. 3C).

As M11L was previously reported to protect against Fas-induced cell killing (59), we assessed the abilities of various virus-encoded antiapoptotic proteins to inhibit the extrinsic pathway of apoptosis. To induce CD95 (Fas) killing, FLAG-tagged Fas ligand was aggregated with the anti-FLAG antibody (32, 53). Notably, in cells treated with Fas ligand and cycloheximide, which is required for Fas-induced killing of MEFs, potent killing was observed (see Fig. S2 in the supplemental material). Expression of M11L, SPPV14, or vaccinia virus B14, a vaccinia virus virulence factor that inhibits IκB kinase (IKK) (26), had no impact upon Fas-induced killing (see Fig. S2). In MEFs, killing by Fas did not appear to be primarily regulated by the Bcl-2 protein family, since the loss of the essential death mediators Bax and Bak made little difference (see Fig. S2).

Having established that SPPV14 is a *bone fide* antiapoptotic protein (Fig. 2 and 3), we next determined if SPPV14 also interfered with NF-κB signaling, since some vBcl-2 proteins, such as vaccinia virus B14, A52, and N1L (2, 15, 26), fold like Bcl-2 but inhibit NF-κB. As expected, a dominant interfering mutant of IκBα effectively blocked activation of NF-κB induced by two cytokines, interleukin 1β (IL-1β) and tumor necrosis factor alpha (TNF-α), when HEK293T cells were cotransfected with a NF-κB reporter plasmid. Although we were able to confirm the ability of B14 to block NF-κB activation in this assay, neither Bcl-2 nor SPPV14 could (Fig. 3D), even though they were expressed. Overall, our results demonstrate that sheeppox virus SPPV14 can effectively inhibit multiple forms of apoptosis induced by the intrinsic (mitochondrial) pathway (Fig. 2 and 3) but does not appear to interfere with death through the extrinsic pathway or with NF-κB activation.

Sheeppox virus SPPV14 inhibits apoptosis during viral infection. Since SPPV14 can effectively inhibit killing triggered by experimentally applied stimuli, but not Fas, we next investigated its ability to inhibit apoptosis during viral infection (Fig. 4 and 5). Wild-type vaccinia virus infects and propagates in a wide range of mammalian cell lines, including Jurkat and HeLa cells. Deletion of the antiapoptotic protein F1L (63) from vaccinia virus results in apoptosis of infected cells, indicated by the activation of the key cell death mediators Bak (Fig. 4A) and Bax (Fig. 5). To determine if SPPV14 could functionally replace F1L and inhibit vaccinia virus-induced apoptosis, we inserted SPPV14 into a F1L-deficient vaccinia virus, and remarkably, SPPV14 was able to completely block Bak (Fig. 4A) and Bax (Fig. 5B and C) activation, thereby maintaining cell viability during infection with vaccinia virus. These findings are further supported by the observation that SPPV14 in the context of vaccinia virus infection also inhibits PARP cleavage (Fig. 5D).

In summary, we have demonstrated that sheeppox virus

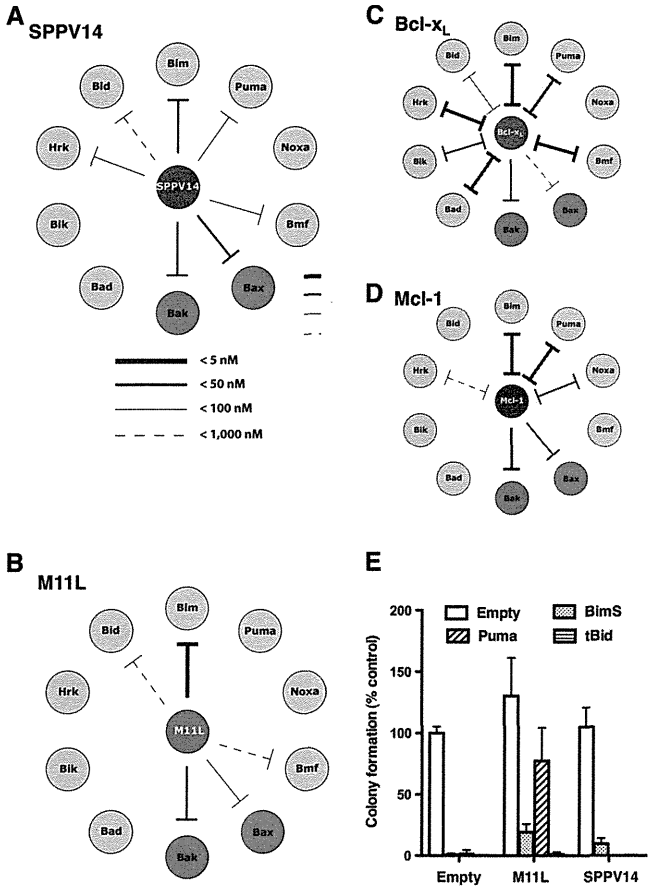

FIG 6 SPPV14 binds a unique set of mammalian proapoptotic proteins. (A to D) SPPV14 binds the BH3 domains of Bak, Bax, and certain BH3-only proteins. The relative binding affinities (IC_{50}) of recombinant SPPV14 (lacking its C terminus) for long BH3 peptides were determined by solution competition assays using the Biacore optical biosensor (9) (Table 1). The relative affinities of the interactions for SPPV14 (A), M11L (40) (B), Bcl-x_L (9) (C), and Mcl-1 (9) (D) are indicated by the thickness of the lines. Absence of a line indicates no binding. (E) Overexpression of Bim_S, Puma, and tBid counters the protection afforded by SPPV14. Shown is colony formation of M11L- or SPPV14-expressing MEFs infected with viruses expressing Bim_S, Puma, tBid, or an empty control. The number of colonies formed is expressed as a proportion of the colonies formed with the empty vector. The data represent means and SD from 2 independent experiments.

SPPV14 counters multiple experimentally applied inducers of apoptosis and appears fully functionally competent even in the context of infection with a distantly related virus, such as vaccinia virus.

SPPV14 interacts with a selective subset of mammalian Bcl-2 proteins. The capacity of most vBcl-2 proteins to inhibit apoptosis depends on the ability to bind and interfere with the action of mammalian proapoptotic proteins (4, 23, 40, 41, 61). Since SPPV14 potently prevented the activation of proapoptotic Bax and Bak (Fig. 4 and 5), we further investigated the molecular basis of Bax and Bak inhibition by testing the ability of SPPV14 to interact with mammalian proapoptotic Bcl-2 proteins. Initially, we evaluated the ability of recombinant SPPV14 to bind the BH3 domains of eight BH3-only proteins, as well as Bax and Bak, via solution competition assays (Fig. 6A and Table 1) (9). Bak and Bax BH3 domains were bound strongly with a 50% inhibitory concentration (IC_{50}) of <50 nM. For the BH3-only proteins, strong binding (IC_{50} < 50 nM) to Bim was observed, whereas other BH3-only proteins, such as Puma, Bmf, Hrk, and Bid, bound more weakly to SPPV14 (Table 1). No binding was detected with Noxa, Bik, or Bad when tested at the highest peptide concentration (2 μM), and these findings were confirmed *in vivo* in immunoprecipitation assays (Fig. 7A) for Bim, Bid, Puma, Bad, and Bmf.

Compared to the binding profiles observed for other prosurvival Bcl-2 proteins (Fig. 6 and Table 1), SPPV14 was found to be unique. Whereas both M11L and SPPV14 engaged Bim, Bak, and Bax, SPPV14 also showed significant affinity for Puma, Hrk, and Bmf (Table 1). In accordance with the *in vitro* binding assay, the BH3-only proteins Bim, tBid, and Puma, which could bind SPPV14, also countered its prosurvival effect when overexpressed in MEFs (Fig. 6E). Unlike SPPV14, M11L cannot bind Puma, and its prosurvival effect was thus not countered by Puma overexpression in MEFs. Moreover, the pattern observed for SPPV14 is distinct from that observed with the two broad classes of mammalian prosurvival Bcl-2 proteins exemplified by Bcl-x_L and Mcl-1 (Fig. 6). The unique pattern observed with SPPV14 may well reflect the specific functional requirements for such an inhibitor in the context of a viral infection.

SPPV14 can functionally antagonize cell death mediated by Bax or Bak. Since SPPV14 can bind both Bax and Bak *in vitro* (Fig. 6) and these findings were confirmed *in vivo* in immunoprecipi-

TABLE 1 Binding affinities of selected prosurvival Bcl-2 proteins for BH3 ligands

BH3 ligand	Binding affinity (IC_{50}[a] in nM)							
	SPPV14	M11L	BHRF1	Bcl-2	Bcl-w	Bcl-x_L	Mcl-1	A1
Bad	>2,000	>1,000	>2,000	16	30	5.3	>100,000	15,000
Bid	341 ± 16	100	42	6,800	40	82	2,100	1
Bik	>2,000	>1,000	>2,000	850	12	43	1,700	58
Bim	26 ± 4	5	<50	2.6	4.3	4.6	2.4	1
Bmf	67 ± 6	100	>2,000	3	9.8	9.7	1,100	180
Hrk	63 ± 6	>1,000	>1,000	320	49	3.7	370	46
Noxa	>2,000	>1,000	>2,000	>100,000	>100,000	>100,000	24	20
Puma	65 ± 1	>1,000	<50	3.3	5.1	6.3	5	1
Bak	46 ± 3	50	NA	>1,000	500	50	10	NA
Bax	32 ± 5	75	NA	100	58	130	12	NA
Bim2A	>1,000	NA	NA	>10,000	>10,000	>10,000	19	520
ABT-737	>1,000	NA	>20,000	3.5	9.5	5.7	>2,000	>2,000

[a] IC_{50}s were determined by solution competition assays using the Biacore optical biosensor (9) and represent means ± SD from 3 independent experiments. NA, not available. Apart from SPPV14, data were taken from references 9, 22, 40* to 42*, and 67*.

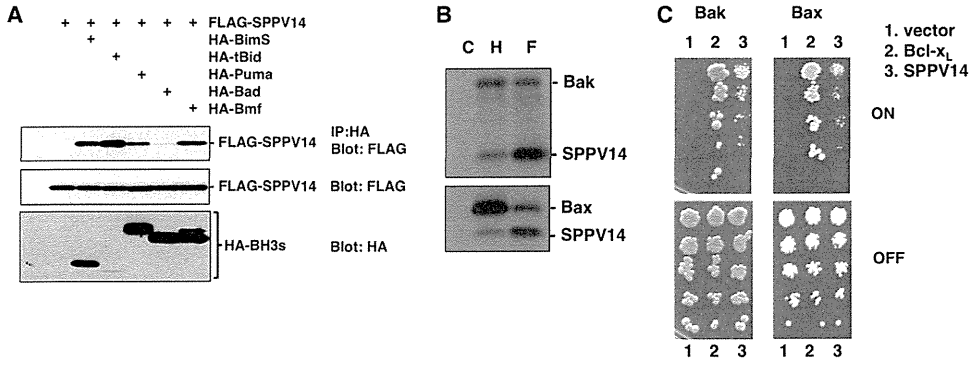

FIG 7 SPPV14 binds both Bak and Bax in mammalian cells and counters growth suppression of yeast by Bax and Bak. (A) Interactions between overexpressed FLAG-SPPV14 and HA-tagged Bim_S, tBid, Puma, Bad, and Bmf were evaluated by coimmunoprecipitation. Equivalent CHAPS-containing 293T cell lysates were immunoprecipitated with antibodies to the HA tag, subjected to SDS-PAGE, and analyzed by Western blotting using anti-FLAG antibody. (B) Interactions between overexpressed FLAG-SPPV14 and HA-tagged Bak or Bax were evaluated by coimmunoprecipitation. Equivalent ^{35}S-labeled CHAPS-containing 293T cell lysates were immunoprecipitated with antibodies to FLAG (F), HA (H), or control (C) tags. (C) SPPV14 counters growth suppression of yeast by Bak and Bax. Yeasts cotransformed with plasmids encoding the indicated prosurvival proteins and Bak or Bax, each under the control of an inducible (GAL) promoter, were spotted onto repressing glucose (OFF) or inducing galactose (ON) plates as 5-fold serial dilutions. The images are representative of 2 independent experiments.

tation assays (Fig. 7B), we next determined if SPPV14 could counter Bax and Bak directly. We utilized a yeast-based assay, where overexpression of Bax or Bak leads to yeast growth arrest (37) that can be overcome by overexpression of mammalian prosurvival Bcl-2 proteins. SPPV14 can counter the growth suppression in yeast cells when either Bax or Bak is overexpressed (Fig. 7C). Thus, we surmise that this most likely reflects direct binding, since yeast cells do not express recognizable Bcl-2 family members. Furthermore, SPPV14 specifically blocks Bax- or Bak-mediated cell death, since expressing SPPV14 in cells deficient in either of the cell death mediators Bak or Bax counters apoptosis (Fig. 8A). Furthermore, when all the endogenous mammalian prosurvival proteins in MEFs were inactivated (Fig. 8B) by a combination of the Bim variant Bim_S2A, which selectively targets Mcl-1 (43), and the BH3 mimetic compound ABT-737 (to target Bcl-2, Bcl-x_L, and Bcl-w and spare SPPV14 [Table 1]) (58), expression of SPPV14 maintained cell viability (Fig. 8C), consistent with the notion that it can directly inhibit Bax or Bak. This capacity to restrain Bax and Bak is presumably dependent on how much SPPV14 is sequestered by those BH3-only proteins that target it (Fig. 6 and Table 1), since overexpression of Bim, tBid, and Puma neutralizes the antiapoptotic effect of SPPV14 (Fig. 6E) in colony-forming assays.

In summary, our studies identified SPPV14 as a novel direct inhibitor of Bax and Bak. It also has a highly distinctive binding profile for the proapoptotic Bcl-2 family proteins expressed in mammals.

DISCUSSION

Apoptosis is a potent defense mechanism deployed by higher organisms against viruses, and in turn, viruses have evolved an astonishing array of strategies to ensure their successful proliferation, propagation, and survival (23, 51). Bcl-2-like proteins from numerous viruses, including structural homologs recently recognized in poxviruses (40, 42), have been shown to be of critical importance for subverting host apoptotic defenses. Consequently, loss of viral Bcl-2 proteins often results in apoptosis upon viral infection, as observed for myxoma virus M11L (59) and vaccinia virus F1L (63).

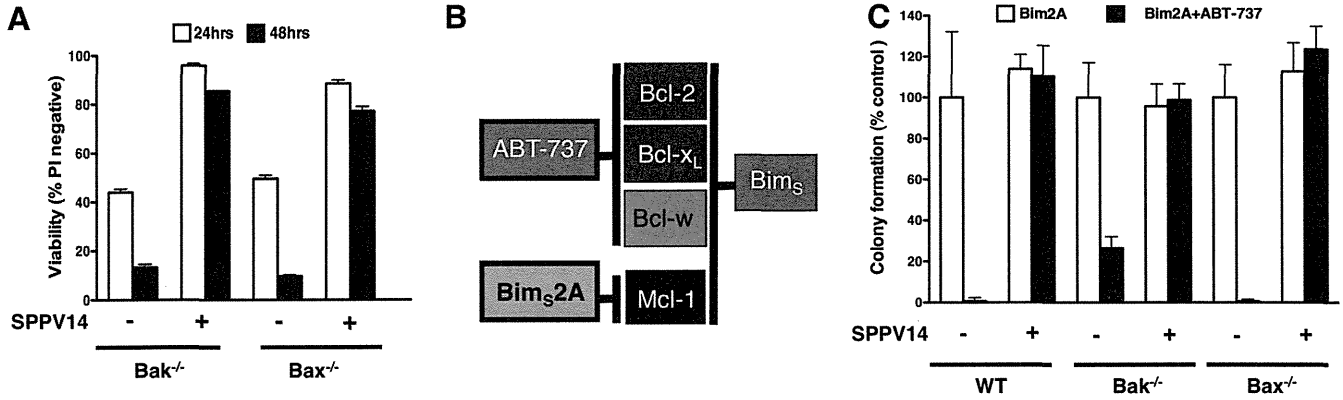

FIG 8 SPPV14 inhibits both Bax and Bak and functionally compensates for endogenous prosurvival Bcl-2. (A) SPPV14 inhibits both Bak- and Bax-mediated apoptosis. Shown is the viability of SPPV14-expressing Bak- or Bax-deficient MEFs treated for 24 h or 48 h with etoposide (10 mM). (B) Selectivity of BH3-only proteins for mammalian prosurvival Bcl-2 proteins (9, 58). (C) SPPV14 potently inhibits apoptosis even if all endogenous mammalian prosurvival Bcl-2 proteins are neutralized. Shown is colony formation of parental or SPPV14-expressing wild-type or Bax- or Bak-deficient MEFs infected with the Mcl-1-selective ligand Bim_S2A (43) and cotreated with ABT-737 (1 μM), a combination that inactivates all endogenous mammalian prosurvival proteins expressed in MEFs (9, 67). The data in panels A and C represent means and SD from 2 independent experiments using a clone of each genotype.

Here, we report the identification and characterization of a novel subgroup of vBcl-2 proteins, the founding members being myxoma virus M11L (25, 40) and vaccinia virus F1L (42, 63). Like the M11L gene, all the novel genes we identified encode putative proteins that bear little primary sequence resemblance to mammalian prosurvival Bcl-2 proteins. Even though the overall sequence similarity to M11L is also low, the critical residues forming the canonical binding grove in M11L (40) were conserved in all six proteins, strongly suggesting the presence of an analogous BH3 binding grove in these proteins (Fig. 1 and 2). Despite the presence of these critical residues, unexpectedly, not all 6 identified M11L orthologs harbored antiapoptotic activity (Fig. 2D). SPV12 (from swinepox virus), gp011L (from shope fibroma virus), and DPV084 (from deerpox virus) did not inhibit etoposide-induced apoptosis when expressed in MEFs. Close inspection of the residues in the putative binding grooves of all six orthologs suggests that four residues, M52, T67, L68, and A71, as a group may determine antiapoptotic activity (see Fig. S1 in the supplemental material). Notably, the only sequence differences between DPV83 and -84 are T25M, A71S, and A101T. With A71 located in the putative binding grove, it is tempting to speculate that the A71S substitution is responsible for the observed difference in antiapoptotic activity. Although the finding that not all six identified M11L orthologs are antiapoptotic was unexpected, it is well established that simple fold conservation in the case of Bcl-2-like proteins is not sufficient for maintaining function. As shown for the vaccinia virus Bcl-2-like proteins A52 and B14 (26), the presence of a Bcl-2 fold does not automatically result in an ability to inhibit Bcl-2-mediated apoptosis. In contrast, both A52 (26) and B14 (10) act on the NF-κB pathway. Similarly, N1L from vaccinia virus also adopts a Bcl-2 fold (2, 12) and acts on NF-κB (7). Importantly, N1L was also shown to inhibit Bcl-2-mediated apoptosis (12), thus displaying dual functionality, which is mediated by two independent sites on the protein (45). It is possible that the three M11L orthologs that were inactive in our apoptosis assays act on NF-κB; however, this remains to be tested experimentally.

In addition to the structure-based sequence analysis, our detailed characterization of sheeppox virus SPPV14 and the previously reported deerpox virus DPV022 (4) support the idea that these viral proteins adopt a Bcl-2-like fold. Like the mammalian prosurvival proteins and myxoma virus M11L, a number of BH3-only proteins can bind SPPV14 (Fig. 6 and Table 1). The binding pattern we observed is unique: Puma can bind and antagonize SPPV14, but not M11L (Fig. 6). Furthermore, SPPV14 can act to directly counter the cell death mediators Bax and Bak, when tested directly (Fig. 7 and 8), in accordance with its ability to bind them (Fig. 6 and Table 1). Considering the similarities in the BH3 domain binding profile and activity against Bax and Bak, the additional ability of SPPV14 to engage Puma, which is absent in M11L, is striking. Among the currently characterized Bcl-2-like proteins from poxviruses, only ORFV125 (65) appears to engage Puma, in addition to Bim, Bik, Hrk, Noxa, and Bax, whereas with F1L (21, 42), N1L (2, 12), and FWPV039 (3, 5), a Puma interaction is not observed. Although the importance of the SPPV14-Puma interaction is currently not established, it is tempting to speculate that, based on the high IC_{50} of 63 nM, the interaction may be functionally relevant.

Functionally, SPPV14 appears to be equipotent to M11L in apoptosis inhibition (Fig. 2 and 3), despite the observed differences in BH3 domain binding. In addition to interactions with Bcl-2 family members (40, 59), M11L has also been reported to form part of the mitochondrial permeability transition pore complex (20) and to intersect with death receptor-mediated apoptosis signaling (59). While it is unclear if SPPV14 also harbors such additional functionality with respect to the mitochondrial permeability transition pore complex, we did not observe an effect of either SPPV14 or M11L on Fas ligand-mediated death signaling (see Fig. S2 in the supplemental material).

In the context of vaccinia virus infection, SPPV14 is able to replace F1L (Fig. 4 and 5) to prevent apoptosis. F1L has been shown to have a highly restricted BH3 binding profile and engages only Bim, Bak, and Bax BH3 domains in biosensor assays (21, 42). Although an interaction with Bax was detected using recombinant protein and peptides, no evidence of a similar interaction in the cellular context has been reported. Functionally, F1L has been shown to engage Bak (48, 61) and Bim (56) and to replace the antiapoptotic activity of Mcl-1 (8), although the precise molecular basis for F1L-mediated apoptosis inhibition remains unclear, with evidence both for (56) and against (18, 50) a role for Bim being reported. Although SPPV14 is able to replace F1L in the context of vaccinia virus, it remains to be established if the mechanism utilized by SPPV14 is similar to the one used by F1L. This is particularly pertinent when considering three issues: first, SPPV14 and F1L ligand binding profiles are substantially different, and second, F1L does not appear to inhibit Bax directly, whereas SPPV14 appears to be M11L-like and to act by neutralizing both Bax and Bak. Third, SPPV14 expression in our experimental system was driven by the strong synthetic poxviral thymidine kinase (17) locus early/late promoter, leading to expression levels and patterns for SPPV14 that are likely to be different from those for endogenous F1L.

Taken together and considering that both vaccinia virus F1L and myxoma virus M11L play key roles for these viruses, we speculate that SPPV14 performs a similar role in sheeppox virus. Key sequence regions in the Bcl-2 family that regulate apoptosis are typically highly conserved. In sheep, Bim harbors two amino acid substitutions at the periphery of the BH3 domain, whereas the Bax BH3 domain is fully conserved, suggesting that at least the SPPV14 interactions with Bim and Bax are likely to be relevant in the context of the sheeppox virus natural host.

By using M11L as bait, we identified a family of novel antiapoptotic factors expressed by poxviruses. Our functional and biophysical characterization of sheeppox virus SPPV14 strongly suggested that SPPV14 adopts a Bcl-2 fold in spite of scant sequence similarity. Interestingly, while SPPV14 seems to play a prominent role in apoptosis inhibition, it does not impact upon the activity of NF-κB, unlike certain other vBcl-2 proteins expressed by vaccinia virus (26). Thus, we anticipate that the detailed characterization of vBcl-2 proteins, such as SPPV14, will continue to unravel the processes that control essential cellular functions in higher organisms.

ACKNOWLEDGMENTS

We thank J. Fletcher, M. Hinds, S. L. Khaw, B. Smith, and M. Yabal for discussions; Abbott Laboratories for ABT-737; F. Battye, J. Blyth, A. Georgiou, H. Ierino, and A. Wardak for excellent technical assistance; and P. Bouillet, D. Fairlie, S. Gerondakis, E. Lee, H. Rabinowich, and A. Strasser for reagents.

Our work is supported by the ARC (fellowship to T.O.), the Cancer Council of Victoria (fellowships to P.M.C.), the Australian National Health and Medical Research Council (program grant 461221; fellow-

ships to P.M.C., D.C.S.H., and M.K.; and IRIISS grant 361646), the Leukemia and Lymphoma Society (SCOR grant 7413; fellowship to M.K.), the Australian Cancer Research Foundation, the Victorian State Government (OIS grant), the Natural Sciences and Engineering Research Council of Canada (graduate scholarship to S.C.), the Alberta Heritage Foundation for Medical Research (studentship to S.C.), the Canadian Institutes of Health Research, the Howard Hughes Medical Institute, and Alberta Innovates Health Solutions. M.B. is a Tier I Canada Research Chair, a Senior Scholar of Alberta Innovates Health Solutions, and a Howard Hughes Medical Institute Scholar in Infection and Parasitology.

REFERENCES

1. **Afonso CL, et al.** 2000. The genome of fowlpox virus. J. Virol. **74**:3815–3831.
2. **Aoyagi M, et al.** 2007. Vaccinia virus N1L protein resembles a B cell lymphoma-2 (Bcl-2) family protein. Protein Sci. **16**:118–124.
3. **Banadyga L, Gerig J, Stewart T, Barry M.** 2007. Fowlpox virus encodes a Bcl-2 homologue that protects cells from apoptotic death through interaction with the proapoptotic protein Bak. J. Virol. **81**:11032–11045.
4. **Banadyga L, et al.** 2010. Deerpox virus encodes an inhibitor of apoptosis that regulates Bak and Bax. J. Virol. **85**:1922–1934.
5. **Banadyga L, Veugelers K, Campbell S, Barry M.** 2009. The fowlpox virus BCL-2 homologue, FPV039, interacts with activated Bax and a discrete subset of BH3-only proteins to inhibit apoptosis. J. Virol. **83**:7085–7098.
6. **Barry M, et al.** 2000. Granzyme B short-circuits the need for caspase 8 activity during granule-mediated cytotoxic T-lymphocyte killing by directly cleaving Bid. Mol. Cell. Biol. **20**:3781–3794.
7. **Bartlett N, Symons JA, Tscharke DC, Smith GL.** 2002. The vaccinia virus N1L protein is an intracellular homodimer that promotes virulence. J. Gen. Virol. **83**:1965–1976.
8. **Campbell S, Hazes B, Kvansakul M, Colman P, Barry M.** 2010. Vaccinia virus F1L interacts with Bak using highly divergent Bcl-2 homology domains and replaces the function of Mcl-1. J. Biol. Chem. **285**:4695–4708.
9. **Chen L, et al.** 2005. Differential targeting of pro-survival Bcl-2 proteins by their BH3-only ligands allows complementary apoptotic function. Mol. Cell **17**:393–403.
10. **Chen RA, Ryzhakov G, Cooray S, Randow F, Smith GL.** 2008. Inhibition of IkappaB kinase by vaccinia virus virulence factor B14. PLoS Pathog. **4**:e22. doi:10.1371/journal.ppat.0040022.
11. **Cleary ML, Smith SD, Sklar J.** 1986. Cloning and structural analysis of cDNAs for *bcl*-2 and a hybrid *bcl*-2/immunoglobulin transcript resulting from the t(14;18) translocation. Cell **47**:19–28.
12. **Cooray S, et al.** 2007. Functional and structural studies of the vaccinia virus virulence factor N1 reveal a Bcl-2-like anti-apoptotic protein. J. Gen. Virol. **88**:1656–1666.
13. **Cuconati A, White E.** 2002. Viral homologs of BCL-2: role of apoptosis in the regulation of virus infection. Genes Dev. **16**:2465–2478.
14. **Dewson G, Snowden RT, Almond JB, Dyer MJ, Cohen GM.** 2003. Conformational change and mitochondrial translocation of Bax accompany proteasome inhibitor-induced apoptosis of chronic lymphocytic leukemic cells. Oncogene **22**:2643–2654.
15. **DiPerna G, et al.** 2004. Poxvirus protein N1L targets the I-kappaB kinase complex, inhibits signaling to NF-kappaB by the tumor necrosis factor superfamily of receptors, and inhibits NF-kappaB and IRF3 signaling by Toll-like receptors. J. Biol. Chem. **279**:36570–36578.
16. **Douglas AE, Corbett KD, Berger JM, McFadden G, Handel TM.** 2007. Structure of M11L: a myxoma virus structural homolog of the apoptosis inhibitor, Bcl-2. Protein Sci. **16**:695–703.
17. **Earl PL, Moss B, Wyatt LS, Carroll MW.** 1998. Generation of recombinant vaccinia viruses, p 16.17.11–16.17.19. *In* Ausubel FM, et al (ed), Current protocols in molecular biology. Wiley Interscience, New York, NY.
18. **Eitz Ferrer P, et al.** 2011. Induction of Noxa-mediated apoptosis by modified vaccinia virus Ankara depends on viral recognition by cytosolic helicases, leading to IRF-3/IFN-beta-dependent induction of pro-apoptotic Noxa. PLoS Pathog. **7**:e1002083. doi:10.1371/journal.ppat.1002083.
19. **Everett H, et al.** 2000. M11L: a novel mitochondria-localized protein of myxoma virus that blocks apoptosis of infected leukocytes. J. Exp. Med. **191**:1487–1498.
20. **Everett H, et al.** 2002. The myxoma poxvirus protein, M11L, prevents apoptosis by direct interaction with the mitochondrial permeability transition pore. J. Exp. Med. **196**:1127–1139.
21. **Fischer SF, et al.** 2006. Modified vaccinia virus Ankara protein F1L is a novel BH3-domain binding protein and acts together with the early viral protein E3L to block virus-associated apoptosis. Cell Death Differ. **13**:109–118.
22. **Fletcher JI, et al.** 2008. Apoptosis is triggered when prosurvival Bcl-2 proteins cannot restrain Bax. Proc. Natl. Acad. Sci. U. S. A. **105**:18081–18087.
23. **Galluzzi L, Brenner C, Morselli E, Touat Z, Kroemer G.** 2008. Viral control of mitochondrial apoptosis. PLoS Pathog. **4**:e1000018. doi:10.1371/journal.ppat.1000018.
24. **Goldmacher VS, et al.** 1999. A cytomegalovirus-encoded mitochondria-localized inhibitor of apoptosis structurally unrelated to bcl-2. Proc. Natl. Acad. Sci. U. S. A. **96**:12536–12541.
25. **Graham KA, Opgenorth A, Upton C, McFadden G.** 1992. Myxoma virus M11L ORF encodes a protein for which cell surface localization is critical in manifestation of viral virulence. Virology **191**:112–124.
26. **Graham SC, et al.** 2008. Vaccinia virus proteins A52 and B14 share a Bcl-2-like fold but have evolved to inhibit NF-kappaB rather than apoptosis. PLoS Pathog. **4**:e1000128. doi:10.1371/journal.ppat.1000128.
27. **Green DR, Kroemer G.** 2004. The pathophysiology of mitochondrial cell death. Science **305**:626–629.
28. **Griffiths GJ, et al.** 1999. Cell damage-induced conformational changes of the pro-apoptotic protein Bak in vivo precede the onset of apoptosis. J. Cell Biol. **144**:903–914.
29. **Hawkins CJ, Wang SL, Hay BA.** 1999. A cloning method to identify caspases and their regulators in yeast: identification of Drosophila IAP1 as an inhibitor of the Drosophila caspase DCP-1. Proc. Natl. Acad. Sci. U. S. A. **96**:2885–2890.
30. **Henderson S, et al.** 1993. Epstein virus-coded BHRF 1 protein, a viral homologue of Bcl-2 protects human B cells from programmed cell death. Proc. Natl. Acad. Sci. U. S. A. **90**:8479–8483.
31. **Hsu Y-T, Youle RJ.** 1998. Bax in murine thymus is a soluble monomeric protein that displays differential detergent-induced conformations. J. Biol. Chem. **273**:10777–10783.
32. **Huang DC, et al.** 1999. Activation of Fas by FasL induces apoptosis by a mechanism that cannot be blocked by Bcl-2 or Bcl-x_L. Proc. Natl. Acad. Sci. U. S. A. **96**:14871–14876.
33. **Huang DCS, Cory S, Strasser A.** 1997. Bcl-2, Bcl-X_L and adenovirus protein E1B19kD are functionally equivalent in their ability to inhibit cell death. Oncogene **14**:405–414.
34. **Huang DCS, O'Reilly LA, Strasser A, Cory S.** 1997. The anti-apoptosis function of Bcl-2 can be genetically separated from its inhibitory effect on cell cycle entry. EMBO J. **16**:4628–4638.
35. **Huang Q, Petros AM, Virgin HW, Fesik SW, Olejniczak ET.** 2002. Solution structure of a Bcl-2 homolog from Kaposi sarcoma virus. Proc. Natl. Acad. Sci. U. S. A. **99**:3428–3433.
36. **Huang Q, Petros AM, Virgin HW, Fesik SW, Olejniczak ET.** 2003. Solution structure of the BHRF1 protein from Epstein-Barr virus, a homolog of human Bcl-2. J. Mol. Biol. **332**:1123–1130.
37. **Jabbour AM, et al.** 2006. Human Bcl-2 cannot directly inhibit the Caenorhabditis elegans Apaf-1 homologue CED-4, but can interact with EGL-1. J. Cell Sci. **119**:2572–2582.
38. **Jurak I, Schumacher U, Simic H, Voigt S, Brune W.** 2008. Murine cytomegalovirus m38.5 protein inhibits Bax-mediated cell death. J. Virol. **82**:4812–4822.
39. **Kinsella TM, Nolan GP.** 1996. Episomal vectors rapidly and stably produce high-titer recombinant retrovirus. Hum. Gene Ther. **7**:1405–1413.
40. **Kvansakul M, et al.** 2007. A structural viral mimic of prosurvival Bcl-2: a pivotal role for sequestering proapoptotic Bax and Bak. Mol. Cell **25**:933–942.
41. **Kvansakul M, et al.** 2010. Structural basis for apoptosis inhibition by Epstein-Barr virus BHRF1. PLoS Pathog. **6**:e1001236. doi:10.1371/journal.ppat.1001236.
42. **Kvansakul M, et al.** 2008. Vaccinia virus anti-apoptotic F1L is a novel Bcl-2-like domain-swapped dimer that binds a highly selective subset of BH3-containing death ligands. Cell Death Differ. **15**:1564–1571.
43. **Lee EF, et al.** 2008. A novel BH3 ligand that selectively targets Mcl-1 reveals that apoptosis can proceed without Mcl-1 degradation. J. Cell Biol. **180**:341–355.
44. **Liu X, Dai S, Zhu Y, Marrack P, Kappler JW.** 2003. The structure of a Bcl-x_L/Bim fragment complex: implications for Bim function. Immunity **19**:341–352.
45. **Maluquer de Motes C, et al.** 2011. Inhibition of apoptosis and NF-

kappaB activation by vaccinia protein N1 occur via distinct binding surfaces and make different contributions to virulence. PLoS Pathog. 7:e1002430. doi:10.1371/journal.ppat.1002430.
46. **O'Connor L, et al.** 1998. Bim: a novel member of the Bcl-2 family that promotes apoptosis. EMBO J. **17**:384–395.
47. **Oltersdorf T, et al.** 2005. An inhibitor of Bcl-2 family proteins induces regression of solid tumours. Nature **435**:677–681.
48. **Postigo A, Cross JR, Downward J, Way M.** 2006. Interaction of F1L with the BH3 domain of Bak is responsible for inhibiting vaccinia-induced apoptosis. Cell Death Differ. **13**:1651–1662.
49. **Postigo A, Martin MC, Dodding MP, Way M.** 2009. Vaccinia-induced epidermal growth factor receptor-MEK signalling and the anti-apoptotic protein F1L synergize to suppress cell death during infection. Cell Microbiol. **11**:1208–1218.
50. **Postigo A, Way M.** 2012. The vaccinia virus-encoded Bcl-2 homologues do not act as direct Bax inhibitors. J. Virol. **86**:203–213.
51. **Roulston A, Marcellus RC, Branton PE.** 1999. Viruses and apoptosis. Annu. Rev. Microbiol. **53**:577–628.
52. **Sarid R, Sato T, Bohenzky RA, Russo JJ, Chang Y.** 1997. Kaposi's sarcoma-associated herpesvirus encodes a functional Bcl-2 homologue. Nat. Med. **3**:293–298.
53. **Schneider P, et al.** 1998. Conversion of membrane-bound Fas(CD95) ligand to its soluble form is associated with downregulation of its proapoptotic activity and loss of liver toxicity. J. Exp. Med. **187**:1205–1213.
54. **Smith CA.** 1995. A novel viral homologue of Bcl-2 and Ced-9. Trends Cell Biol. **5**:344.
55. **Strasser A.** 2005. The role of BH3-only proteins in the immune system. Nat. Rev. Immunol. **5**:189–200.
56. **Taylor JM, Quilty D, Banadyga L, Barry M.** 2006. The vaccinia virus protein F1L interacts with Bim and inhibits activation of the proapoptotic protein Bax. J. Biol. Chem. **281**:39728–39739.
57. **Thompson JD, Higgins DG, Gibson TJ.** 1994. CLUSTAL W: improving the sensitivity of progressive multiple sequence alignment through sequence weighting, position-specific gap penalties and weight matrix choice. Nucleic Acids Res. **22**:4673–4680.
58. **van Delft MF, et al.** 2006. The BH3 mimetic ABT-737 targets selective Bcl-2 proteins and efficiently induces apoptosis via Bak/Bax if Mcl-1 is neutralized. Cancer Cell **10**:389–399.
59. **Wang G, et al.** 2004. Myxoma virus M11L prevents apoptosis through constitutive interaction with Bak. J. Virol. **78**:7097–7111.
60. **Wang GQ, et al.** 2001. Resistance to granzyme B-mediated cytochrome *c* release in Bak-deficient cells. J. Exp. Med. **194**:1325–1337.
61. **Wasilenko ST, Banadyga L, Bond D, Barry M.** 2005. The vaccinia virus F1L protein interacts with the proapoptotic protein Bak and inhibits Bak activation. J. Virol. **79**:14031–14043.
62. **Wasilenko ST, Meyers AF, Vander Helm K, Barry M.** 2001. Vaccinia virus infection disarms the mitochondrion-mediated pathway of the apoptotic cascade by modulating the permeability transition pore. J. Virol. **75**:11437–11448.
63. **Wasilenko ST, Stewart TL, Meyers AF, Barry M.** 2003. Vaccinia virus encodes a previously uncharacterized mitochondrial-associated inhibitor of apoptosis. Proc. Natl. Acad. Sci. U. S. A. **100**:14345–14350.
64. **Westphal D, et al.** 2007. A novel Bcl-2-like inhibitor of apoptosis is encoded by the parapoxvirus ORF virus. J. Virol. **81**:7178–7188.
65. **Westphal D, et al.** 2009. The orf virus inhibitor of apoptosis functions in a Bcl-2-like manner, binding and neutralizing a set of BH3-only proteins and active Bax. Apoptosis **14**:1317–1330.
66. **White E, et al.** 1992. The 19-kilodalton adenovirus E1B transforming protein inhibits programmed cell death and prevents cytolysis by tumor necrosis factor α. Mol. Cell. Biol. **12**:2570–2580.
67. **Willis SN, et al.** 2005. Pro-apoptotic Bak is sequestered by Mcl-1 and Bcl-xL, but not Bcl-2, until displaced by BH3-only proteins. Genes Dev. **19**:1294–1305.
68. **Youle RJ, Strasser A.** 2008. The BCL-2 protein family: opposing activities that mediate cell death. Nat. Rev. Mol. Cell Biol. **9**:47–59.

Immunity
Article

A Cluster of Interferon-γ-Inducible p65 GTPases Plays a Critical Role in Host Defense against *Toxoplasma gondii*

Masahiro Yamamoto,[1,2,3,4,7,10,*] Megumi Okuyama,[1,10] Ji Su Ma,[1,2,3,4] Taishi Kimura,[1,2] Naganori Kamiyama,[1,2,3,4] Hiroyuki Saiga,[1] Jun Ohshima,[1,2,3,4] Miwa Sasai,[4] Hisako Kayama,[1,2,7] Toru Okamoto,[5,8] David C.S. Huang,[8] Dominique Soldati-Favre,[9] Kyoji Horie,[6] Junji Takeda,[6] and Kiyoshi Takeda[1,2,7,*]

[1]Department of Microbiology and Immunology, Graduate School of Medicine
[2]Laboratory of Mucosal Immunology, WPI Immunology Frontier Research Center
[3]Laboratory of Immunoparasitology, WPI Immunology Frontier Research Center
[4]Department of Immunoparasitology, Research Institute for Microbial Diseases
[5]Department of Molecular Virology, Research Institute for Microbial Diseases
[6]Department of Social and Environmental Medicine, Graduate School of Medicine
Osaka University, Yamadaoka, Suita, Osaka 565-0871, Japan
[7]Core Research for Evolutional Science and Technology, Japan Science and Technology Agency, Saitama 332-0012, Japan
[8]The Walter and Eliza Hall Institute of Medical Research and Department of Medical Biology, University of Melbourne, Parkville, VIC 3052, Australia
[9]Department of Microbiology and Molecular Medicine, CMU, University of Geneva, 1211 Geneva 4, Switzerland
[10]These authors contributed equally to this work
*Correspondence: myamamoto@biken.osaka-u.ac.jp (M.Y.), ktakeda@ongene.med.osaka-u.ac.jp (K.T.)
http://dx.doi.org/10.1016/j.immuni.2012.06.009

SUMMARY

Interferon-γ (IFN-γ) is essential for host defense against intracellular pathogens. Stimulation of innate immune cells by IFN-γ upregulates ~2,000 effector genes such as immunity-related GTPases including p65 guanylate-binding protein (Gbp) family genes. We show that a cluster of *Gbp* genes was required for host cellular immunity against the intracellular parasite *Toxoplasma gondii*. We generated mice deficient for all six *Gbp* genes located on chromosome 3 (*Gbp*^{chr3}) by targeted chromosome engineering. Mice lacking *Gbp*^{chr3} were highly susceptible to *T. gondii* infection, resulting in increased parasite burden in immune organs. Furthermore, *Gbp*^{chr3}-deleted macrophages were defective in IFN-γ-mediated suppression of *T. gondii* intracellular growth and recruitment of IFN-γ-inducible p47 GTPase Irgb6 to the parasitophorous vacuole. In addition, some members of Gbp^{chr3} restored the protective response against *T. gondii* in *Gbp*^{chr3}-deleted cells. Our results suggest that Gbp^{chr3} play a pivotal role in anti-*T. gondii* host defense by controlling IFN-γ-mediated Irgb6-dependent cellular innate immunity.

INTRODUCTION

Interferon-γ (IFN-γ) is an important T helper 1 (Th1) cell cytokine that strongly suppresses the growth and survival of intracellular pathogens (Boehm et al., 1997). Stimulation of innate immune cells such as macrophages and dendritic cells by IFN-γ results in robust gene expression of a number of effector molecules. These include immunity-related GTPases such as the Mx proteins, immunity-related p47 GTPases (Irgs), and p65 guanylate-binding proteins (Gbps) (Shenoy et al., 2007; Taylor et al., 2004). Mx proteins have been shown to participate in host defense against RNA viruses such as influenza and vesicular stomatitis virus (Sadler and Williams, 2008). Among the Irgs, mice deficient in Irgm1 (Lrg-47) are highly susceptible to *Listeria*, *Salmonella*, and mycobacteria (Deretic, 2006; MacMicking, 2004). Furthermore, Gbps have recently been shown to induce antibacterial responses involving phagocytic oxidases, autophagic effectors, and inflammasome (Kim et al., 2011; Shenoy et al., 2012). Thus, IFN-γ-inducible immunity-related GTPases play pivotal roles in antiviral and antibacterial immune systems.

Toxoplasma gondii is an obligatory intracellular protozoan parasite that infects virtually all warm-blooded vertebrates including human and mouse (Boothroyd, 2009; Israelski and Remington, 1993). Infection of immunocompromised individuals such as those suffering from AIDS or those being treated with chemotherapy often leads to fatal toxoplasmosis encephalitis (Montoya and Remington, 2008). Innate immune cells, which recognize microbial components mainly via Toll-like receptors (TLRs) and the chemokine receptor CCR5, are essential in controlling *T. gondii* infection via the production of proinflammatory cytokines such as interleukin-12 (IL-12) (Aliberti et al., 2003; Hunter and Remington, 1995; Yarovinsky and Sher, 2006). IL-12 potentiates polarization of naive T cells to Th1 cells, from which IFN-γ is produced in an antigen-dependent fashion (Trinchieri, 2003; Whitmarsh et al., 2011). IFN-γ-inducible GTPases are also important for the inhibition of *T. gondii* growth by IFN-γ. Mice lacking Irgm1, Irgd (Irg-47), Irgm3 (Igtp), or Irga6 (Iigp1) are susceptible to acute and chronic infection (Collazo et al., 2001; Howard et al., 2011; Taylor et al., 2000). IRGs are recruited to the parasitophorous vacuole (PV), a membrane formed during invasion that is maintained to surround the intracellular

replicating parasites. Accumulation of Irgs eventually leads to disruption of the integrity of the PV membranes (Howard et al., 2011; Ling et al., 2006; Taylor et al., 2007; Zhao et al., 2008).

Not only Irgs but also Gbps are known to accumulate around the PV shortly after *T. gondii* invasion (Degrandi et al., 2007). Moreover, because virulent strains of *T. gondii* inhibit the recruitment of Gbps around the PV (Degrandi et al., 2007; Virreira Winter et al., 2011), Gbps are considered anti-*T. gondii* defensive factors. Among Gbps, Gbp1 and Gbp2 are reported to modulate cellular proliferation (Gorbacheva et al., 2002; Guenzi et al., 2001). In addition, Gbp1 is involved in the regulation of matrix metalloproteinase 1 in cancer cell lines (Guenzi et al., 2003; Li et al., 2011). Although in vitro studies have been reported, the physiological protective role of Gbps against *T. gondii* remains uncertain. The mouse genome carries 13 *Gbp* genes (11 active members and 2 pseudogenes) that are organized in clusters and share a high degree of homology (Kresse et al., 2008). Six and seven family members are tandemly aligned on chromosomes 3 and 5, respectively (Kresse et al., 2008). Such a complex configuration has hampered in vivo investigation of the *Gbp* genes through genetic approaches.

To elucidate the in vivo functional contribution of the Gbps to host defense against *T. gondii*, we have generated mice lacking the entire cluster of *Gbp*s on chromosome 3 (Gbp^{chr3}) by Cre-loxP-based chromosome engineering. Gbp^{chr3}-deleted mice were highly susceptible to *T. gondii* infection with a considerably increased parasite burden in tissues. Furthermore, Gbp^{chr3}-deleted macrophages showed defective suppression of parasite growth in response to IFN-γ. Although parasite infection-induced production of oxidants and proinflammatory cytokines as well as autophagy-related 4b (Atg4b) recruitment to the parasites were normal, IFN-γ-induced disruption of the PV membrane and localization of Irgs such as Irgb6 and Irgb10 to the PV were compromised in Gbp^{chr3}-deleted cells. Moreover, endogenous Gbps colocalized and interacted with Irgb6. The reintroduction of *Gbp1*, *Gbp5*, or *Gbp7* into Gbp^{chr3}-deleted cells *partially* restored the IFN-γ-dependent anti-*T. gondii* response. Taken together, these results demonstrate that this cluster of Gbps has a defensive function against *T. gondii* by positively regulating IFN-γ-inducible Irgb6-dependent cellular innate immunity.

RESULTS

Generation of Mice Lacking the Entire *Gbp* Locus on Chromosome 3

To assess the anti-*T. gondii* immunity of Gbp^{chr3} in vivo, we generated embryonic stem (ES) cells possessing loxP sites at the most proximal and distal loci from the centromere in the gene cluster (*Gbp5* and *Gbp2ps*, respectively) by sequential conventional gene targeting methods (Figure 1A and Figure S1 available online). Deletion of the entire Gbp^{chr3} locus spanning 173 kb was achieved by crossing the F1 mice with CAG-Cre transgenic mice and was confirmed by Southern blotting and PCR (Figures 1B and 1C). Gbp^{chr3}-deleted mice were successfully obtained by intercrossing heterozygous mice, were born at the expected Mendelian ratio, and were healthy and normal in specific-pathogen-free conditions (Figure 1D). Under nonstimulated conditions, Gbp^{chr3}-deleted mice showed normal parameters of cellular immunity (Figure S1H). To test whether the expression of Gbp^{chr3} was correctly ablated in Gbp^{chr3}-deleted cells, we confirmed by quantitative RT-PCR that the mRNAs derived from Gbp^{chr3} (*Gbp1*, *Gbp2*, *Gbp3*, *Gbp5*, *Gbp7*, and *Gbp2ps*) were not induced in response to IFN-γ in Gbp^{chr3}-deleted cells (Figure 1E). On the other hand, mRNAs for the Gbps on chromosome 5 (*Gbp4*, *Gbp6*, *Gbp8*, *Gbp9*, *Gbp10*, and *Gbp11*) were normally induced. We further analyzed Gbp^{chr3} expression by protein immunoblotting and found that Gbp1, Gbp2, and Gbp5 proteins were not detected. A weak signal was observed when we performed blotting with Gbp1-5 monoclonal antibodies that are raised against amino acids 1–300 mapping at the N terminus of human GBP1 and that recognize a shared epitope among Gbp1, Gbp2, Gbp3, Gbp4, and Gbp5. Expression of the gene encoding Gbp4, which is not disrupted in Gbp^{chr3}-deleted cells, could account for this weak signal (Figure 1F).

Gbp^{chr3} Confer Resistance to *T. gondii* In Vivo

First, mice lacking *Gbp2ps* alone or deficient in both *Gbp2ps* and *Gbp5* were infected intraperitoneally with the avirulent *T. gondii* strain ME49 and shown to exhibit survival rates similar to those of wild-type mice (Figures S1C and S1F). In contrast, infection of Gbp^{chr3}-deleted mice revealed that these mutant mice were highly prone to die after *T. gondii* infection (Figure 2A). Because Gbp1 and Gbp5 were recently shown to be involved in host defense against *Listeria monocytogenes* (Kim et al., 2011; Shenoy et al., 2007), we challenged Gbp^{chr3}-deleted mice with *L. monocytogenes* by intraperitoneal injection. Wild-type and Gbp^{chr3}-deleted mice exhibited comparable bacterial burdens in tissues and survival rate (Figures S2A and S2B). To monitor the course of infection more accurately, we generated transgenic ME49 *T. gondii* expressing luciferase and monitored the kinetics by in vivo imaging in wild-type and Gbp^{chr3}-deleted mice infected with 10^2 parasites. Significant increases in parasite number were observed at days 7, 8, and 9 in Gbp^{chr3}-deleted mice compared with those in wild-type mice (Figures 2B and S2C). We next compared parasite burdens in organs from the infected mice. The parasite load showed an excellent correlation with luciferase counts in vitro (Figures S2D and S2E). We collected the spleens and mesenteric lymph nodes from wild-type or Gbp^{chr3}-deleted mice 9 days after a challenge with luciferase-expressing parasites and calculated the parasite numbers according to the luciferase signal. The parasite load in the tissues originating from Gbp^{chr3}-deleted mice was markedly elevated in comparison with that from wild-type mice (Figure 2C). Taken together, these findings demonstrate that Gbp^{chr3} protects against the spreading and proliferation of *T. gondii* in vivo.

Next we examined immune responses during parasite infection in wild-type and Gbp^{chr3}-deleted mice. IL-12 is important for the development of type I immunity, in which IFN-γ-producing $CD4^+$ and $CD8^+$ T cells play central roles for anti-*T. gondii* responses (Hunter et al., 1995). The concentrations of IL-12p40 and IFN-γ measured in sera were similarly increased in wild-type and Gbp^{chr3}-deleted mice infected with *T. gondii* (Figure 2D). Furthermore, cellularity in spleens and IFN-γ production from splenic $CD4^+$ and $CD8^+$ T cells in response to anti-CD3 was comparable in wild-type and Gbp^{chr3}-deleted mice (Figures 2E and S2F), suggesting that the high susceptibility to *T. gondii* in Gbp^{chr3}-deleted mice was not due to defects in production of IL-12 or IFN-γ or in T cell responses.

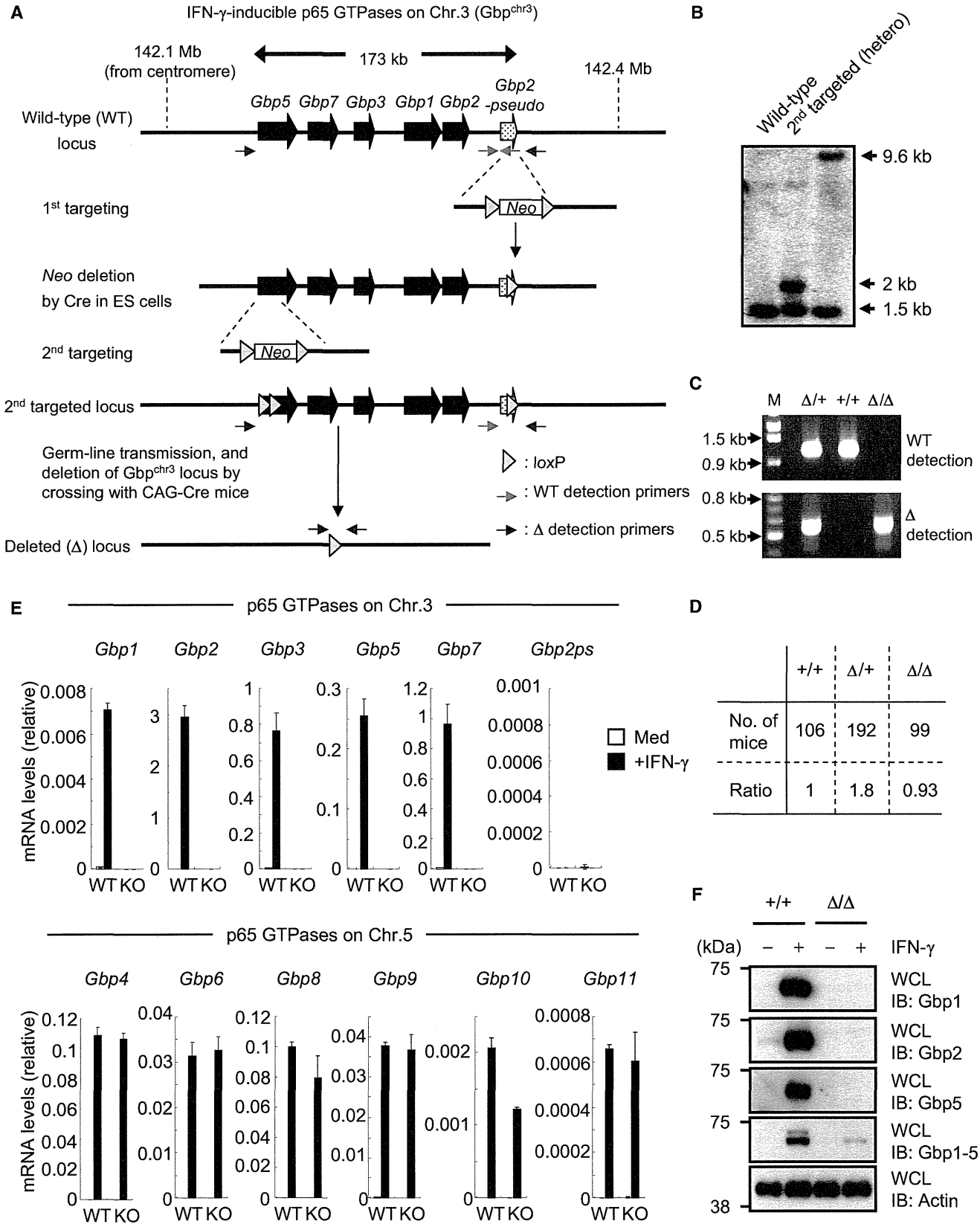
A
IFN-γ-inducible p65 GTPases on Chr.3 (Gbp^chr3)
142.1 Mb
(from centromere)
173 kb
142.4 Mb
Gbp5 Gbp7 Gbp3 Gbp1 Gbp2 Gbp2 -pseudo
Wild-type (WT) locus
1st targeting
Neo
Neo deletion by Cre in ES cells
2nd targeting
Neo
2nd targeted locus
Germ-line transmission, and deletion of Gbp^chr3 locus by crossing with CAG-Cre mice
Deleted (Δ) locus
: loxP
: WT detection primers
: Δ detection primers
B
Wild-type
2nd targeted (hetero)
9.6 kb
2 kb
1.5 kb
C
M Δ/+ +/+ Δ/Δ
1.5 kb
0.9 kb
WT detection
0.8 kb
0.5 kb
Δ detection
D
+/+ Δ/+ Δ/Δ
No. of mice 106 192 99
Ratio 1 1.8 0.93
E
p65 GTPases on Chr.3
Gbp1 Gbp2 Gbp3 Gbp5 Gbp7 Gbp2ps
mRNA levels (relative)
Med
+IFN-γ
WT KO
p65 GTPases on Chr.5
Gbp4 Gbp6 Gbp8 Gbp9 Gbp10 Gbp11
F
+/+ Δ/Δ
(kDa) − + − + IFN-γ
75
WCL IB: Gbp1
WCL IB: Gbp2
WCL IB: Gbp5
WCL IB: Gbp1-5
38
WCL IB: Actin

Gbp^{chr3} Are Essential for IFN-γ-Induced Reduction of *T. gondii* Infection in Macrophages

Macrophages play a vital role in IFN-γ-mediated cellular innate immunity against *T. gondii* (Suzuki et al., 1988). Peritoneal macrophages represent a major cell type targeted by the parasite at the early stage after intraperitoneal infection (Jensen et al., 2011). To analyze the impact of *Gbp*^{chr3} deficiency in this cell type, we infected wild-type or *Gbp*^{chr3}-deleted peritoneal macrophages with *T. gondii* expressing luciferase in the presence of IFN-γ and assessed the luciferase units at 1, 12, 24, 36, or 48 hr postinfection (Figure 3A). We observed higher luciferase emissions in *Gbp*^{chr3}-deleted cells than in wild-type cells at all time points tested except for 1 hr. Next, we analyzed the IFN-γ-dependent reduction of parasite burden by counting parasite numbers and the luciferase units in macrophages and mouse embryonic fibroblasts (MEFs) from wild-type or *Gbp*^{chr3}-deleted mice. The dose-dependent reduction of parasite numbers and luciferase signals in both cell types lacking *Gbp*^{chr3} was less pronounced than that in wild-type cells (Figures 3B and S3A). On the other hand, costimulation of tumor necrosis factor-α (TNF-α), which is known to strongly enhance antitoxoplasmal activity in macrophage in combination with IFN-γ (Sibley et al., 1991), abrogated the difference between wild-type and *Gbp*^{chr3}-deleted cells (Figure S3B). These data suggested a selective impairment in IFN-γ-mediated reduction of parasite burden.

IFN-γ leads to inhibition of *T. gondii* proliferation and promotes its clearance from macrophages (Ling et al., 2006). To measure clearance, we next used confocal microscopy to compare the degree of parasite infection and growth in macrophages isolated from wild-type or *Gbp*^{chr3}-deleted mice. At 5 hr postinfection, the percentage of cells infected with the parasites was comparable between wild-type and *Gbp*^{chr3}-deleted mice (Figure 3C). In contrast, the infection rate of IFN-γ-stimulated macrophages from *Gbp*^{chr3}-deleted mice was remarkably higher than that from wild-type cells after 20 hr (Figures 3C, 3D, and S3C). Next, we compared the rate of parasite replication in wild-type and *Gbp*^{chr3}-deleted macrophages in the presence of IFN-γ by counting the parasite numbers per PV. In *Gbp*^{chr3}-deleted cells, the number of parasites per PV was modestly increased compared with that in wild-type cells (Figures 3D and 3E), indicating that Gbp^{chr3} are not only required for clearance but also inhibit parasite replication in IFN-γ-stimulated macrophages.

Impact of Gbp^{chr3} Deficiency on IFN-γ-Mediated Anti-*T. gondii* Response

Among Gbp^{chr3}, Gbp1 and Gbp7 have been shown to participate in antibacterial host defense by inducing an oxidative response and recruiting autophagy effectors such as Atg4b to *L. monocytogenes* and *Mycobacterium bovis* (Kim et al., 2011). To test whether these mechanisms also apply to anti-*T. gondii* defense, we first measured IFN-γ-induced oxide ion (O^{2-}) production in wild-type or *Gbp*^{chr3}-deleted cells infected with *T. gondii* (Figure 4A). The O^{2-} production in *Gbp*^{chr3}-deleted macrophages was normally enhanced. Next, we examined Atg4b recruitment to the parasite by confocal microscopy. As observed for pathogenic bacteria, Atg4b colocalized with intracellular *T. gondii* in wild-type cells. The increased recruitment of Atg4b to parasites in *Gbp*^{chr3}-deleted macrophages was not altered during the course of infection (Figures 4B and S4A). Taken together, these results suggest that the anti-*T. gondii* action of Gbp^{chr3} operates independently of O^{2-} and Atg4b recruitment.

IFN-γ is also known to augment proinflammatory cytokine production in response to TLR ligands, and *T. gondii* possesses a profilin that can serve as a TLR11 ligand called profilin-like molecule (Plattner et al., 2008; Yarovinsky et al., 2005). We analyzed the production of proinflammatory cytokines in macrophages. Production of tumor necrosis factor α, IL-6, and IL-12p40 in IFN-γ-treated *Gbp*^{chr3}-deleted cells in response to *T. gondii* infection or lipopolysaccharide (LPS) was normal (Figure S4B), indicating that Gbp^{chr3} are dispensable for IFN-γ-mediated production of proinflammatory cytokines.

Because nitric oxide (NO) was previously reported to inhibit *T. gondii* replication in vitro (Adams et al., 1990), we assessed NO production in wild-type and *Gbp*^{chr3}-deleted cells. Nonstimulated, *T. gondii*-infected, or LPS-treated macrophages from *Gbp*^{chr3}-deleted mice produced similar concentrations of nitrite ion (NO^{2-}) compared with that produced by wild-type cells (Figure S4C). Furthermore, hepatic expression of iNOS mRNAs was unchanged between wild-type and *Gbp*^{chr3}-deleted mice in *T. gondii* infection (Figure S4D). In spite of normal NO production in *Gbp*^{chr3}-deleted macrophages (Figure S4C), the inhibition of the parasite replication was modestly impaired by the *Gbp*^{chr3} deficiency (Figure 3E). To examine whether NO is involved in inhibition of parasite replication in *Gbp*^{chr3}-deleted cells, we compared the replication in *Gbp*^{chr3}-deleted cells between those untreated and those treated with aminoguanidine (AG), an NO inhibitor (Figure 4C). Although the infection rate was not affected at all, AG-treated *Gbp*^{chr3}-deleted cells contained significantly larger numbers of the parasites per vacuole than control cells, indicating that NO indeed plays a major role in inhibition of *T. gondii* replication in *Gbp*^{chr3}-deleted macrophages in vitro. To further determine relative importance of Gbp^{chr3} in the IFN-γ-dependent anti-*T. gondii* response in vivo, we compared parasite burdens and the survival rate of wild-type and

Figure 1. Generation of *Gbp*^{chr3}-Deleted Mice

(A) The gene targeting strategy for *Gbp*^{chr3} locus by chromosome engineering.

(B) Southern blot analysis of offspring from the heterozygote intercrosses. Genomic DNA was extracted from mouse tails, digested with KpnI and PstI, electrophoresed, and hybridized with the radiolabelled probe indicated in Figure S1G. Southern blotting resulted in a 1.5 kb band for wild-type locus, a 2.0 kb band for deleted (Δ) locus, and 9.6 kb for second targeted locus.

(C) PCR detection of mice with homozygous deletion of *Gbp*^{chr3} locus. Primers used are denoted in (A).

(D) Numbers of offspring by intercross of heterozygous (Δ/+) mice.

(E) Quantitative PCR analysis of the expression of the indicated Gbp mRNA in wild-type (WT) or *Gbp*^{chr3}-deleted (KO) peritoneal macrophages unstimulated or stimulated with 100 ng/ml IFN-γ.

(F) Peritoneal macrophages treated with 100 ng/ml IFN-γ for 24 hr were lysed. The lysates were detected by protein immunoblot with the indicated Abs.

Data are representative of two (B, C, E) and three (F) independent experiments. See also Figure S1.

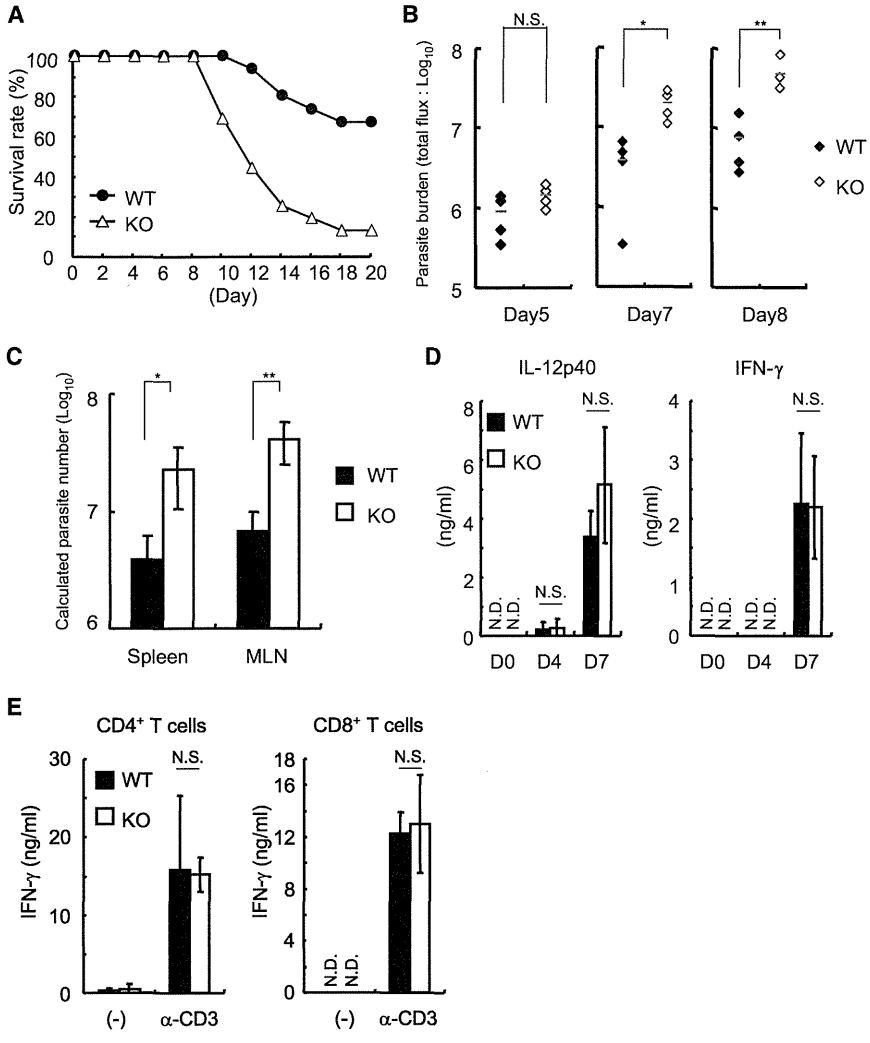

Figure 2. *Gbp*^{chr3}-Deleted Mice Are Highly Susceptible to *T. gondii*

(A) Wild-type (n = 15) or *Gbp*^{chr3}-deleted (KO) (n = 16) mice were infected with 1 × 10^2 *T. gondii*, and the survival rates were monitored for 20 days.

(B) Total photon emission analysis from wild-type or *Gbp*^{chr3}-deleted mice (n = 4 per group) infected with 1 × 10^2 ME49 *T. gondii* luciferase-expressing parasites at days 5, 7, or 8 after infection. The flux (photons/s/cm^2/sr) was determined as a measure of parasite burden. *p < 0.01, **p < 0.02.

(C) Quantification of parasites in indicated tissues from 4 mice per group at day 9 postinfection by the standard curve in Figure S2. Indicated values are means ± SD of quadruplicates. *p < 0.005, **p < 0.03.

(D) Sera were taken from indicated mice (n = 4 per group) at the indicated time postinfection of 1 × 10^2 *T. gondii*. Serum concentrations of the indicated cytokines were determined by ELISA.

(E) Splenic CD4$^+$ or CD8$^+$ T cells from indicated mice (n = 4 per group) at day 7 postinfection of 1 × 10^2 *T. gondii* were cultured in the presence of 5 μg/ml plate-bound anti-CD3 for 24 hr. Concentration of IFN-γ in the culture supernatants was measured by ELISA. Indicated values are means ± SD of triplicates.

N.D., not detected; N.S., not significant. Data are representative of three (C) and two (B, D, E) independent experiments. Data in (A) are pooled from three independent experiments with five or six mice per group. See also Figure S2.

Gbp^{chr3}-deleted mice treated with anti-IFN-γ (Figures 4D and 4E). Although the mortality was not increased by anti-IFN-γ treatment in *Gbp*^{chr3}-deleted mice (Figure 4D), *Gbp*^{chr3}-deleted mice treated with anti-IFN-γ displayed much higher parasite burdens than did control IgG-treated groups (Figure 4E). These results indicated that Gbp^{chr3} do not fully account for the IFN-γ-dependent anti-*T. gondii* immunity in vitro and in vivo.

Impaired Disruption of the PV Membrane in *Gbp*^{chr3}-Deleted Macrophages

Gbp^{chr3} deficiency resulted in compromised IFN-γ-induced clearance of *T. gondii* in macrophages (Figure 3). The killing by IFN-γ-activated macrophages is accompanied by blebbing of the PV membrane shortly after parasite entry (Ling et al., 2006; Zhao et al., 2008). Therefore, we examined by electron microcopy the morphology of the parasite PV membrane in wild-type and *Gbp*^{chr3}-deleted macrophages 6 hr postinfection. Blebbing and vesiculation were easily detectable in the vicinity of the parasite PV membrane in wild-type cells (Figure 5A). In sharp contrast, in *Gbp*^{chr3}-deleted cells the parasites were surrounded by a continuous intact PV membrane (Figure 5B), suggesting that Gbps affect IFN-γ-induced clearance of *T. gondii* shortly after invasion. Moreover, 24 hr postinfection, a markedly increased number of dead parasites with damaged parasite membranes or no PV membranes were observed in wild-type cells compared with those in *Gbp*^{chr3}-deleted cells (Figure 5C and data not shown).

Defective Irgb6 Recruitment to PVs in *Gbp*^{chr3}-Deleted Macrophages

A previous study demonstrated that macrophages lacking the autophagy protein Atg5 exhibit defective blebbing of the *T. gondii* PV (Zhao et al., 2008), which is reminiscent of the phenotype observed in *Gbp*^{chr3}-deleted cells (Figure 5B). Atg5 has been reported to be required for the recruitment of Irga6 to the PV (Zhao et al., 2008). Irgs including Irga6 (also known as IIGP1), Irgb6 (TGTP), and Irgb10 were shown to be phosphorylated and dampened by *T. gondii* ROP18, a parasite-secreted kinase that acts as a virulence effector molecule (Fentress et al., 2010; Steinfeldt et al., 2010). The CTG strain of *T. gondii* produces an extremely low *ROP18* mRNA expression (Boothroyd and Dubremetz, 2008; Saeij et al., 2006; Taylor et al., 2006); hence the CTG parasites as well as ME49 are permissive for Irg recruitment to the PV membrane (Saeij et al., 2006; Taylor et al., 2006). By using the CTG strain expressing luciferase, we found that the IFN-γ-dependent decrease in CTG parasites was impaired in *Gbp*^{chr3}-deleted macrophages (Figure 6A),

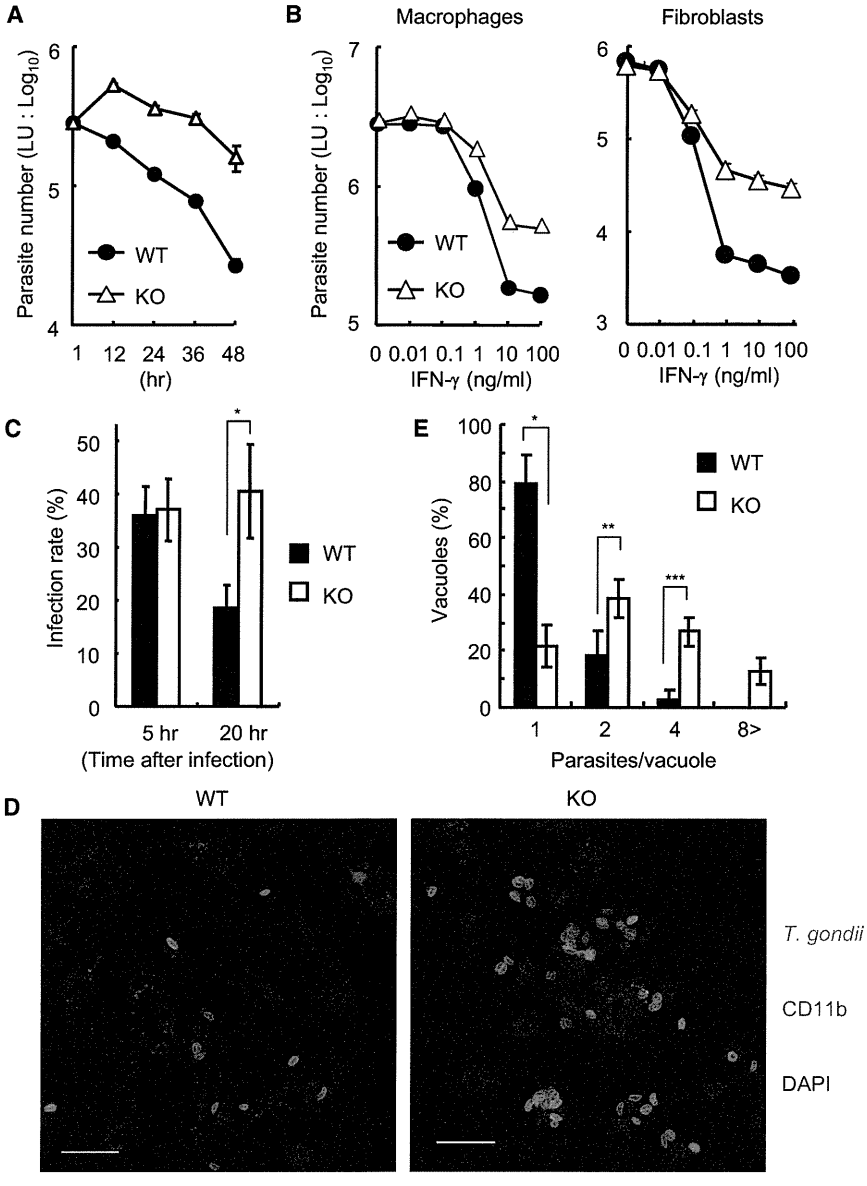

Figure 3. Impaired IFN-γ-Mediated Parasite Clearance in *Gbp*^{chr3}-Deleted Macrophages

(A) Wild-type (WT) and *Gbp*^{chr3}-deleted (KO) peritoneal macrophages were treated with 100 ng/ml IFN-γ for 24 hr. IFN-γ-treated cells were infected with ME49 *T. gondii* expressing lucifease (moi = 0.5) and harvested at the indicated point postinfection. The luciferase units (LU) were assayed with the lysates. Indicated values are means ± SD of triplicates.

(B) WT and KO peritoneal macrophages or MEFs were untreated or treated with the indicated concentrations of IFN-γ for 24 hr. Untreated or IFN-γ-treated cells were infected with ME49 *T. gondii* expressing luciferase (moi = 0.5) and harvested at 36 hr postinfection. The LU were assayed with the lysates. Indicated values are means ± SD of triplicates.

(C) The percentage of WT and KO macrophages containing at least one *T. gondii* parasite at the indicated points postinfection. Indicated values are means ± SD of triplicates. $^{**}p < 0.03$.

(D) WT and KO peritoneal macrophages were treated with 100 ng/ml IFN-γ for 24 hr. IFN-γ-treated cells were infected with ME49 *T. gondii* (moi = 0.5), fixed at 24 hr postinfection, and stained with rabbit anti-*T. gondii* (Alexa 488, green) or rat anti-Cd11b (Alexa 594, red). Scale bars represent 20 μm.

(E) The number of *T. gondii* parasites per vacuole in WT or KO macrophages at 24 hr postinfection. Indicated values are means ± SD of triplicates. $^{*}p < 0.02$, $^{**}p < 0.04$, $^{***}p < 0.002$.

Data are representative of five (A), three (B), and two (D) independent experiments. Data in (C) and (E) are pooled from three independent experiments in which almost 150 cells and 140 vacuoles were counted, respectively. See also Figure S3.

suggesting that Irg-mediated immunity could be affected by *Gbp*^{chr3} deficiency. To test this possibility, we first analyzed the amount of Irgb6 protein expression in IFN-γ-treated macrophages. Similar amounts of Irgb6 protein were induced in wild-type and *Gbp*^{chr3}-deleted cells upon stimulation by IFN-γ (Figure 6B). Next, we tested the recruitment of Irgb6 to the PV by confocal microscopy. At 6 hr postinfection, Irgb6 was detectable at the PV in wild-type cells. In contrast, the recruitment of Irgb6 was severely impaired in *Gbp*^{chr3}-deleted macrophages (Figure 6C). The extent of Irgb6 recruitment was analyzed at 2, 4, and 6 hr postinfection. Compared with that in wild-type cells, the percentage of Irgb6-positive parasites in *Gbp*^{chr3}-deleted cells was significantly lower at every time point analyzed (Figure 6D). In addition to Irgb6, we tested the recruitment of other Irgs such as Irgb10, Irga6, and Irgm3 (Figure S5). The recruitment of Irgb10 to the PV was also impaired in *Gbp*^{chr3}-deleted cells (Figure S5A), whereas that of Irga6 was comparable between wild-type and *Gbp*^{chr3}-deleted cells (Figures S5B and S5C). We failed to observe the accumulation of Irgm3 to the PVs even in IFN-γ-stimulated wild-type cells (data not shown). Taken together, these results suggest that Gbp^{chr3} are required for recruitment of Irgb6 and Irgb10 to the PV of *T. gondii* in IFN-γ-activated macrophages.

Gbps Interact with Irgb6

In a previous study, an overexpressed green fluorescent protein (GFP)-Gbp1 fusion protein was shown to colocalize with endogenous Irgb6 and *T. gondii* parasites (Virreira Winter et al., 2011). We confirmed these observations with endogenous proteins by costaining for anti-Gbp1-5 and anti-Irgb6 in wild-type macrophages infected with *T. gondii* (Figure 6E). Furthermore, intensity profile analysis revealed that the signals for both proteins were detected at almost the same sites (Figure 6F). Then, we assessed the interaction between Gbps and Irgb6 in endogenous settings. Immunoprecipitation with anti-Gbp1-5 coprecipitated Irgb6 in IFN-γ-stimulated macrophages, and the amount of Irgb6 coimmunoprecipitated was markedly increased upon *T. gondii* infection (Figure 6G). These results suggest that the

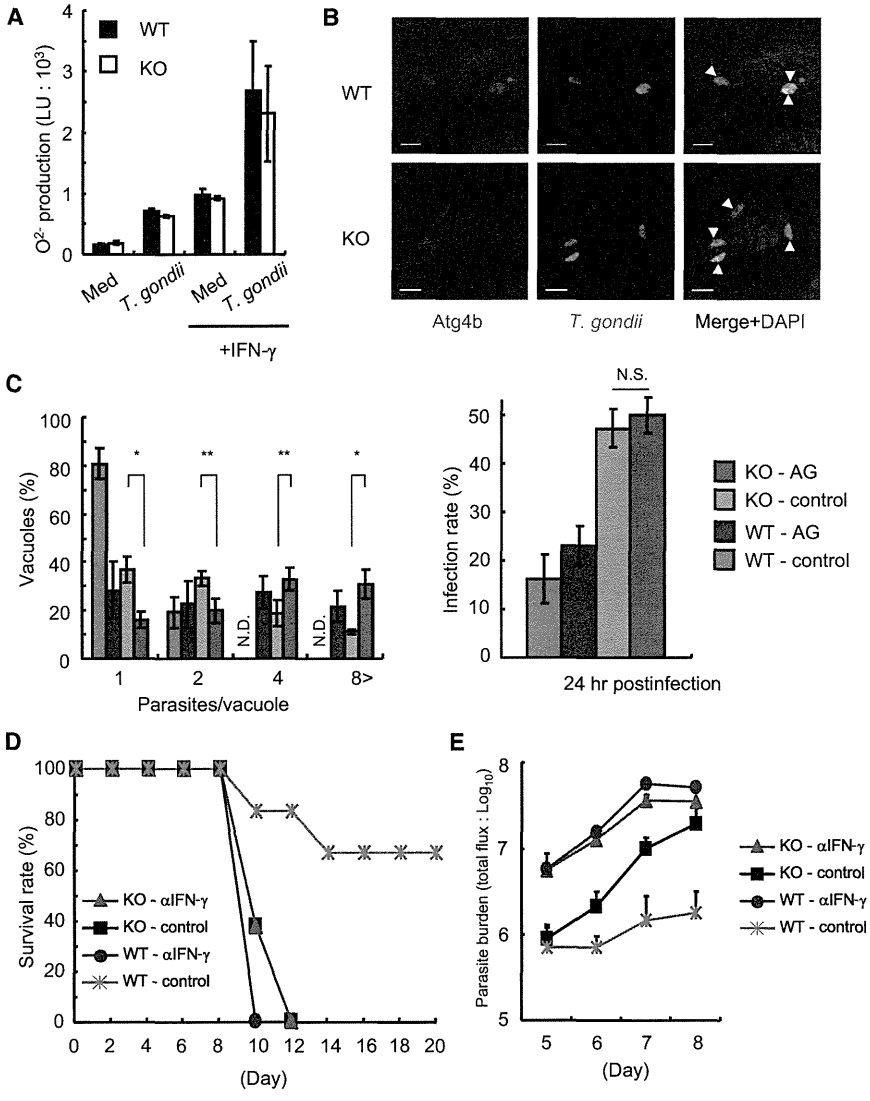

Figure 4. Assessment of IFN-γ-Dependent Responses in *Gbp*^{chr3}-Deleted Mice

(A) Wild-type (WT) and *Gbp*^{chr3}-deleted (KO) peritoneal macrophages were treated with 100 ng/ml IFN-γ for 24 hr. Untreated or IFN-γ-treated cells were uninfected or infected with ME49 *T. gondii* (moi = 0.5) for 24 hr. Concentration (light unit; LU) of O^{2-} in cells was measured with an O^{2-}-specific chemiluminescence reagent by luminometer. Indicated values are means ± SD of triplicates.

(B) WT and KO peritoneal macrophages were treated with 100 ng/ml IFN-γ for 24 hr. IFN-γ-treated cells were infected with ME49 *T. gondii* (moi = 0.5), fixed at 6 hr postinfection, and stained with mouse anti-*T. gondii* (Alexa 488, green) or rabbit anti-Atg4b (Alexa 594, red). Scale bars represent 5 μm.

(C) WT and KO peritoneal macrophages were untreated or treated with 100 ng/ml IFN-γ for 24 hr in the presence or absence of 100 μM AG. Cells were infected with ME49 *T. gondii* expressing luciferase (moi = 0.5). Left: The number of parasites per vacuole in WT or KO macrophages at 24 hr postinfection is shown. Indicated values are means ± SD of triplicates. *p < 0.01, **p < 0.03. Right: The percentage of WT and KO macrophages containing at least one parasite at 24 hr postinfection is shown. Indicated values are means ± SD of triplicates. N.S., not significant.

(D) Mice (WT intraperitoneally injected with 1 mg of anti-IFN-γ [n = 5] or with control IgG [n = 6] and KO with anti-IFN-γ [n = 8] or with control IgG [n = 8] before 1 day of the parasite challenge) were intraperitoneally infected with 1 × 10^2 *T. gondii*, and the survival rates were monitored for 20 days.

(E) Total photon emission analysis from indicated mice (n = 4 per group) infected with 1 × 10^2 ME49 *T. gondii* luciferase-expressing parasites at days 5, 6, 7, or 8 after infection. The flux (photons/s/cm^2/sr) was determined as a measure of parasite burden.

Data are representative of two (A, B, C, E) independent experiments. Data in (D) are pooled from two independent experiments. See also Figure S4.

association of Irgb6 with Gbps is fundamental to the defective Irgb6 recruitment to *T. gondii* in *Gbp*^{chr3}-deleted cells.

Gbp^{chr3} Participate Differentially in Anti-*T. gondii* Defense

Although the Gbps share a high degree of homology (Kresse et al., 2008), variation in the amino acid sequence among Gbp^{chr3} is greater than that among Gbp^{chr5}. It is uncertain whether the five active members of *Gbp*^{chr3} (*Gbp1*, *Gbp2*, *Gbp3*, *Gbp5*, and *Gbp7*) similarly or differentially contribute to the anti-*T. gondii* cellular immunity. To address this question, we cloned each Gbp into drug-responsive retroviral expression vectors and expressed them in a tightly doxycycline-dependent manner in *Gbp*^{chr3}-deleted primary MEFs (Figure 7A). Parasite clearance in the absence or presence of IFN-γ was then tested in these transduced cells. Reintroduction of *Gbp1*, *Gbp5*, or *Gbp7* into *Gbp*^{chr3}-deleted MEFs *partially* restored the IFN-γ-dependent clearance of *T. gondii* compared with wild-type cells (Figures 3B and 7B), indicating that these proteins possess common and compensatory functions in the anti-*T. gondii* immune response. Taken together, our results show that Gbp^{chr3} play a pivotal role in IFN-γ-mediated cellular innate immune response to *T. gondii*.

DISCUSSION

This study makes use of targeted chromosome engineering to provide genetic evidence for the critical role of Gbp^{chr3} in defense against *T. gondii* infection. Mice lacking *Gbp*^{chr3} were highly susceptible to *T. gondii* infection, and *Gbp*^{chr3}-deleted macrophages are defective in IFN-γ-mediated inhibition of intracellular parasite growth.

The Gbp-mediated cellular immune mechanism was previously reported to be pleiotropic and implicated IFN-γ-inducible phagocytic oxidative killing and the trafficking of antimicrobial peptides to autophagolysosomes by their interaction with NADPH oxidase subunits and autophagy-related molecules such as Atg4b, respectively (Kim et al., 2011). In this previous

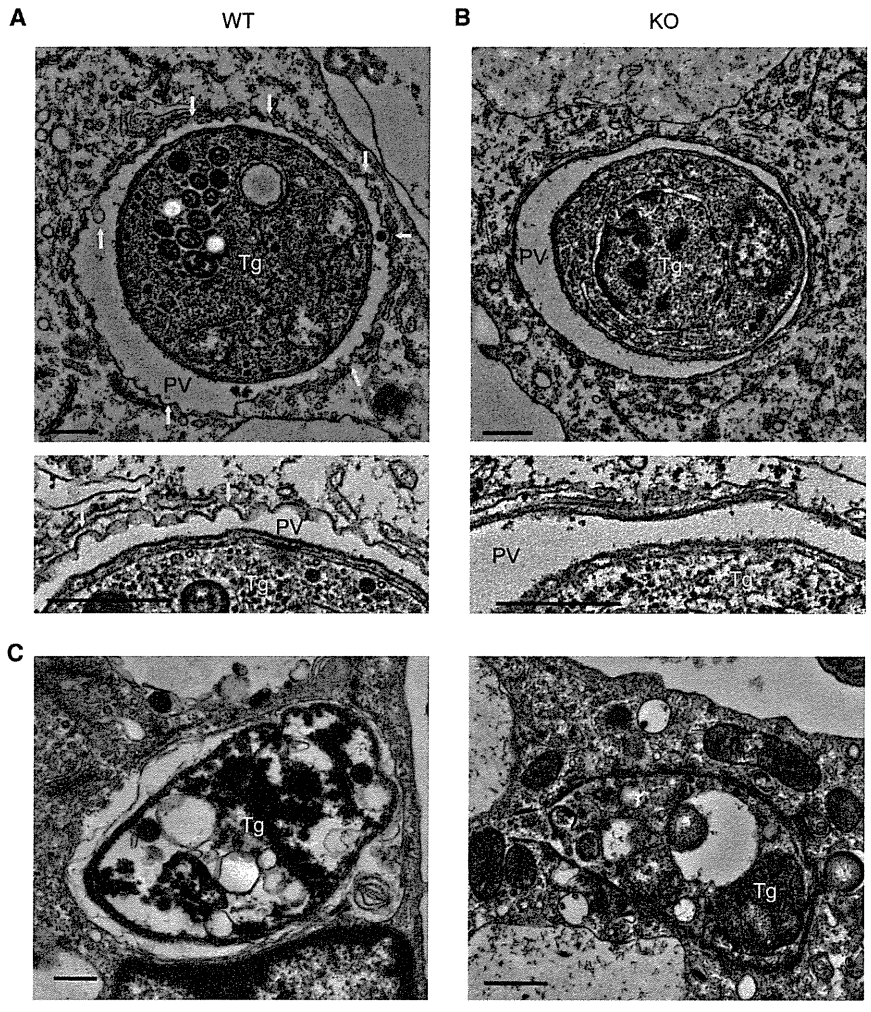

Figure 5. Electron Microscopic Analysis of IFN-γ-Activated Macrophages
(A and B) Wild-type (A) or *Gbp*^{chr3}-deleted (B) peritoneal macrophages were treated with 100 ng/ml IFN-γ for 24 hr. IFN-γ-treated cells were infected with ME49 *T. gondii* (moi = 0.5) for 6 hr and then analyzed by electron microscopy. The lower images are enlarged views from the upper images. Tg, *T. gondii*; PV, parasitophorous vacuole. Arrows indicate protrusive blebs inside or outside parasitophorous vacuoles (A).
(C) Images of dead parasites at 24 hr postinfection in IFN-γ-treated wild-type cells. Tg, *T. gondii*.
Scale bars represent 0.2 μm. Data are representative of two independent experiments.

study, Gbp function was mainly tested with dominant-negative forms of Gbps or small interfering RNA-mediated knockdown (Kim et al., 2011). Here, we observed normal O^{2-} production in response to IFN-γ stimulation and Atg4b recruitment to PVs in *Gbp*^{chr3}-deleted macrophages. Instead, we found that *Gbp*^{chr3} deficiency affected recruitment of some Irgs to *T. gondii*-infected macrophages. The discrepancy between the two studies might be explained by the different pathogens, or alternatively, it is possible that the other cluster of *Gbp*s on chromosome 5 (*Gbp*^{chr5}) may play a compensatory role in the oxidative and autophagy-related responses.

Blebbing of the PV membrane was not induced in IFN-γ-activated macrophages lacking *Gbp*^{chr3}, which is akin to that observed in Atg5-deficient cells (Zhao et al., 2008). The similar phenotypes of both mutant mice prompted us to examine the localization of Irgs during *T. gondii* infection. *Gbp*^{chr3} deficiency impaired accumulation of Irgb6 and Irgb10 but not of Irga6 around the parasite, suggesting that the Gbps play a major role in some Irg recruitment. This model contrasts with previous studies suggesting that Irgs control localization of Gbps based on the fact that IFN-γ prestimulation is required for the localization of overexpressed Gbps to *T. gondii* (Degrandi et al., 2007), and that Gbp2 localization is altered in Irgm-deficient cells (Traver et al., 2011). Considering that Gbps and Irgs participate in the anti-*T. gondii* response in close proximity, it is possible that the two families of IFN-γ-inducible GTPases mutually control their localization, at least in part, through physical association. Given that the number of IRGs and GBPs varies among species (2 IRGs and 7 GBPs in human versus 23 Irgs and 13 Gbps in mouse) (Kresse et al., 2008; Shenoy et al., 2007), evolutionary pressure to increase or decrease the number and variety of IRGs could influence the repertoire of GBPs. Furthermore, virulent *T. gondii* strains such as RH are capable of evading recognition by Irgs via the action of the virulence factor ROP18 that phosphorylates the Irgs (Degrandi et al., 2007; Fentress et al., 2010; Steinfeldt et al., 2010; Virreira Winter et al., 2011). In addition, virulent *T. gondii* also prevents the accumulation of Gbps (Virreira Winter et al., 2011). Taken together, ROP18 phosphorylation of Irgs could affect the interaction with Gbps, promoting their dissociation from the parasites. In terms of the kinetics of the recruitment of Irgb6, given that *Gbp*^{chr3} deficiency affected the later phase rather than the early stage, Gbp^{chr3} might play a role in persistence of Irgb6 on PVs in the later stage. Alternatively, other factors including Gbp^{chr5} might also participate in the Irgb6 recruitment in the early phase of infection. Whether deficiency of either *Gbp*^{chr3} or *Gbp*^{chr5} (or both) also affects the localization of other Irgs such as Irgm and Irgd deserves further investigation. Despite the fact that Irgb6 and Irgb10 are shown to be phosphorylated by ROP18 in vitro (strongly indicating the defensive roles of these Irgs) (Fentress et al., 2010), their in vivo functions in immunity to *T. gondii* should still be assessed and confirmed under physiological conditions via mice lacking these Irgs.

The impaired inhibition of *T. gondii* replication in *Gbp*^{chr3}-deleted cells prompted us to investigate the effect of NO on the *Gbp*^{chr3}-dependent resistance to *T. gondii* in vitro. We found that the presence or absence of NO did not affect parasite clearance; the rate of macrophages infected with *T. gondii* was not altered by addition of the NO inhibitor. Given the collaboration

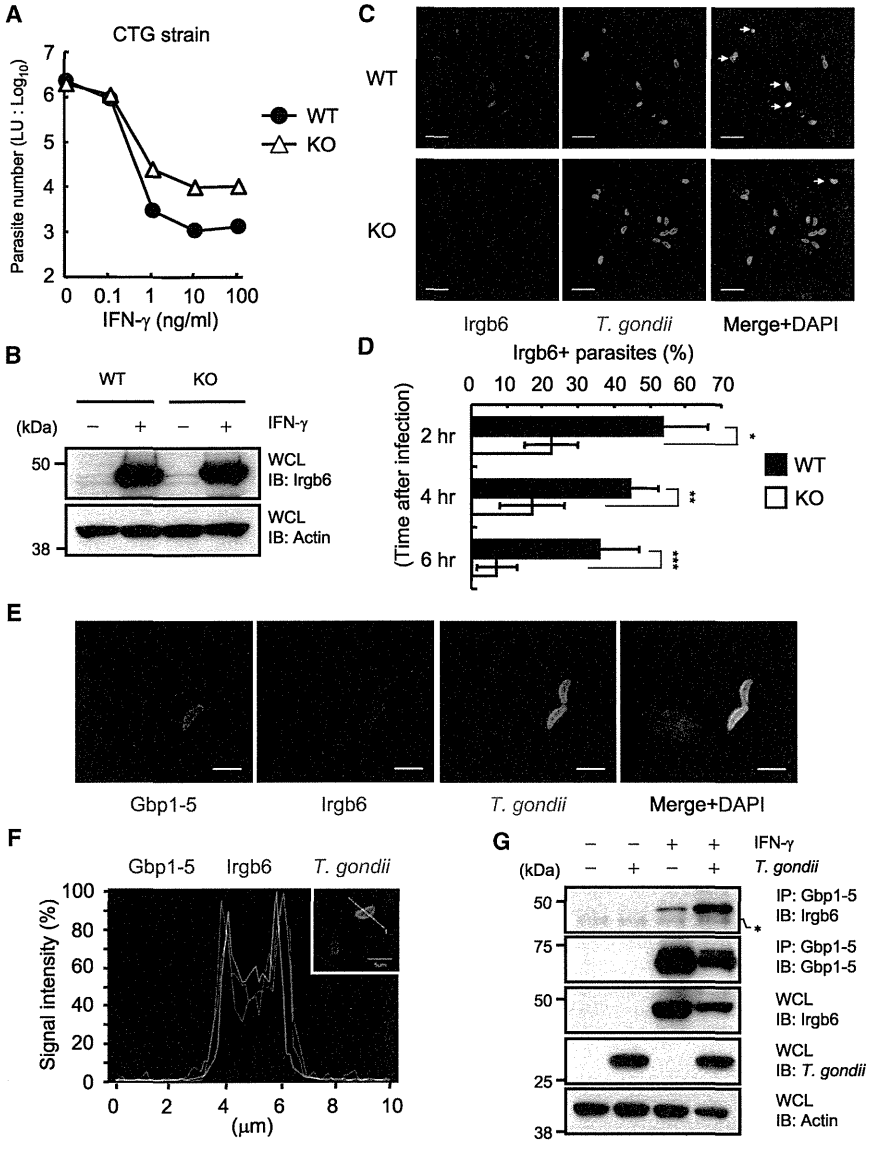

Figure 6. Defective Irgb6 Recruitment in *Gbp*^{chr3}-Deleted Macrophages

(A) Wild-type (WT) and *Gbp*^{chr3}-deleted (KO) peritoneal macrophages were untreated or treated with the indicated concentrations of IFN-γ for 24 hr. Untreated or IFN-γ-treated cells were infected with CTG *T. gondii* expressing luciferase (moi = 0.5) and harvested at 36 hr postinfection. The luciferase units (LU) were assayed with the lysates. Indicated values are means ± SD of triplicates.

(B) Peritoneal macrophages treated with 100 ng/ml IFN-γ for 24 hr were lysed. The lysates were detected by protein immunoblot with the indicated Abs.

(C) WT and KO peritoneal macrophages were treated with 100 ng/ml IFN-γ for 24 hr. IFN-γ-treated cells were infected with ME49 *T. gondii* (moi = 0.5), fixed at 6 hr postinfection, and incubated with rabbit anti-*T. gondii* (Alexa 488, green) or goat anti-Irgb6 (Alexa 594, red). Scale bars represent 10 μm. Arrows indicate colocalization of Irgb6 with *T. gondii*.

(D) The percentage of WT and KO macrophages positive for Irgb6 staining at the indicated points postinfection. Indicated values are means ± SD of triplicates. *$p < 0.03$, **$p < 0.005$, ***$p < 0.004$.

(E and F) Peritoneal macrophages were treated with 100 ng/ml IFN-γ for 24 hr. IFN-γ-treated cells were infected with ME49 *T. gondii* (moi = 0.5), fixed at 6 hr postinfection, and incubated with rabbit anti-*T. gondii* (Alexa 488, green), goat anti-Irgb6 (Alexa 594, red), or mouse anti-Gbp1-5 (Alexa 647, magenta). The samples were analyzed by confocal microscopy and subsequent intensity profile (F). Scale bars represent 5 μm. The signal intensities of each color on the 10 μm white line on the parasites are shown.

(G) Peritoneal macrophages treated with 100 ng/ml IFN-γ for 24 hr were lysed. The lysates were immunoprecipitated with anti-Gbp1-5 and detected by protein immunoblot with the indicated antibodies. Asterisk indicates nonspecific.

Data are representative of two (A, B) or three (C, D, E, F, G) independent experiments. Data in (D) are pooled from three independent experiments, in which almost 150 cells at each time point were counted. See also Figure S5.

of Irg and Gbp, the NO-independent role of Gbp^{chr3} may be parallel to the NO-independent effect of Irg on *T. gondii* clearance (Collazo et al., 2002). In contrast, the presence of Gbp^{chr3} had a modest effect on the inhibition of *T. gondii* replication, which critically involves NO, because *Gbp*^{chr3}-deleted macrophages contained larger numbers of the parasites per PV. Because there is no direct evidence indicating a role of Irg in the suppression of *T. gondii* replication to date, these data may be indicative of an unknown Irg-independent mechanism(s) of Gbp^{chr3} to promote the NO-mediated inhibition of the parasite replication in vitro. Nevertheless, considering that iNOS deficiency has a minor effect on early resistance in vivo (Scharton-Kersten et al., 1997), the high susceptibility in acute *T. gondii* infection in *Gbp*^{chr3}-deleted mice might be due to the defective parasite clearance dependent on some Irgs. Given the relative significance of Gbp^{chr3} in IFN-γ-dependent anti-*T. gondii* responses, the fact that anti-IFN-γ treatment in *Gbp*^{chr3}-deleted mice resulted in enhanced parasite burdens in vivo suggests that additional IFN-γ-inducible effector(s) controls early resistance to the parasite. On the other hand, *Gbp*^{chr3}-deleted mice treated with anti-IFN-γ displayed similar survival rate of mice with control IgG. The apparent disparity might be because anti-IFN-γ blocked IFN-γ-dependent anti-*T. gondii* response, leading not only to high parasite burdens but also to immune pathology mediated by massive and dysregulated doses of IFN-γ at the terminal phase of *T. gondii* infection (Nguyen et al., 2003). In addition, costimulation of TNF-α with IFN-γ resulted in incomparable inhibition of the parasite growth and abolished the Gbp^{chr3}-mediated effect. Although NO concentration in TNF-α and IFN-γ-treated macrophages was markedly higher than that in cells stimulated with IFN-γ alone, further investigation is required to determine whether only the difference of NO

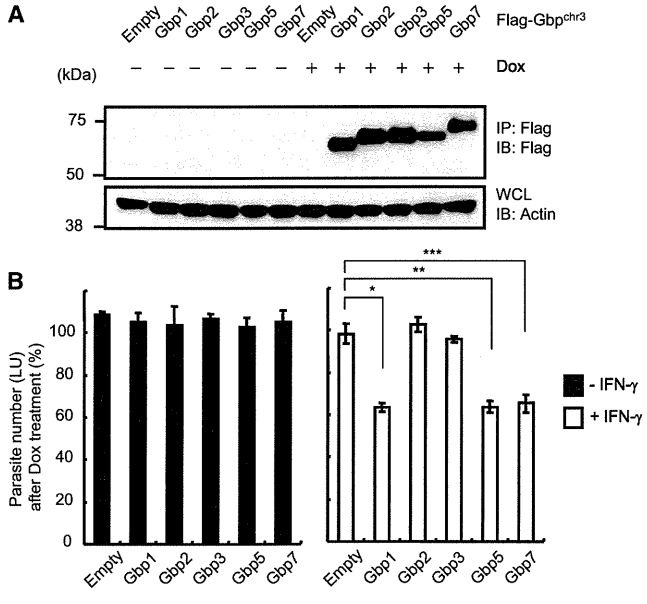

Figure 7. Individual Participation of Gbp^{chr3} in IFN-γ-Dependent Inhibition of *T. gondii* Growth

(A) Retroviral vectors encoding the indicated Flag-tagged Gbps were stably introduced in *Gbp*^{chr3}-deleted (KO) primary MEFs. The transfected MEFs were treated with or without 1 μg/ml doxycycline (Dox) for 24 hr and lysed. The lysates were immunoprecipitated with anti-Flag and detected by protein immunoblot with the indicated antibodies.

(B) The KO MEFs transfected with indicated Gbps were unstimulated or stimulated with 100 ng/ml of IFN-γ for 24 hr with or without 1 μg/ml Dox. Cells were infected with ME49 *T. gondii* parasites expressing luciferase (moi = 0.5) for 36 hr, and the luciferase units (LU) were analyzed. The percentages of the activities after each Gbp induction with Dox over those without Dox (no Gbp induction) in nonstimulated (left) or stimulated (right) cells were shown. Indicated values are means ± SD of triplicates.

Data are representative of two independent experiments. *, **, ***$p < 0.001$.

concentration or other NO-independent effects such as autophagy and augmentation of phagocytic activity accounts for the enhanced protective effect (Keller et al., 2011; Langermans et al., 1992; Leenen et al., 1994).

Gbp1, Gbp5, and Gbp7, but not Gbp2 or Gbp3, were able to restore, albeit not fully, the killing activity by IFN-γ in *Gbp*^{chr3}-deleted MEFs, indicating that Gbp^{chr3} contribute differentially to the anti-*T. gondii* host defense mechanism. This is consistent with a previous finding that knockdown of some Gbps abrogates IFN-γ-dependent suppression of bacterial growth (Kim et al., 2011). In the context of the functional redundancy within Gbp^{chr3}, we observed that mice lacking *Gbp5*, or *Gbp5* and *Gbp2ps*, were resistant to *T. gondii* infection, suggesting that *Gbp5* deficiency may be compensated for by other *Gbp*^{chr3}-encoded proteins such as Gbp1 and Gbp7. On the other hand, mice lacking Gbp1 alone are susceptible to *L. monocytogenes* and *M. bovis*. Interestingly, Gbp5 has recently been shown to play a key role in the host defense in *L. monocytogenes* infection, indicating the nonredundant function of Gbp1 and Gbp5 in the antibacterial response (Kim et al., 2011; Shenoy et al., 2012). In contrast, our *Gbp*^{chr3}-deleted mice displayed resistance to *L. monocytogenes*. This discrepancy may reflect different modes of infection (e.g., oral versus intraperitoneal infections in the previous and current studies, respectively) or utilization of different mice strains (*Gbp1* or *Gbp5* singly deficient mice in previous studies and *Gbp*^{chr3}-deleted mice in this study) (Kim et al., 2011; Shenoy et al., 2012). Moreover, we could not exclude the possibility that Gbp^{chr3} other than *Gbp1* and *Gbp5* play a negative role in Gbp1- and Gbp5-mediated anti-*Listeria* response. It remains to be seen whether deficiency of Gbp1 alone would be sufficient to disrupt the anti-*T. gondii* defense system, but it is nevertheless plausible that each member of Gbp^{chr3} may play a differential role to combat distinct types of pathogens. Given that Gbp2 associates with Gbp1 (Virreira Winter et al., 2011), Gbp2 (and Gbp3) might play a role in host defense against other pathogens or have an additional anti-*T. gondii* effect in the presence of other Gbp^{chr3}. Considering that *Gbp*^{chr3}-deleted cells lack a large genetic region, there is an inherant risk that the phenotype observed in *Gbp*^{chr3}-deleted mice could be unrelated to Irg. Although we adopted in vitro retroviral transfection for the restoration of each Gbp in this study, none of Gbp^{chr3} failed to fully restore the effect of IFN-γ. It remains unclear whether the failure is due to limit of the transfection method or due to nonredundancy among Gbp^{chr3} except for Gbp5. In vivo transgenic reconstitution of the region by an artificial chromosome such as BAC and YAC should be utilized to reveal a role of each Gbp specifically participating in antiparasite in vivo responses in the future (Copeland et al., 2001).

In conclusion, our genetic study with *Gbp*^{chr3}-deleted mice has established that Gbp^{chr3} are required for IFN-γ-mediated host defense against *T. gondii* by regulating Irgb6 recruitment to the parasite. To understand the functions of this family of IFN-γ-inducible p65 GTPases fully, future studies will have to include the second cluster, Gbp^{chr5}, and will need to investigate the effect of these proteins in defense against a broader range of parasites, as well as against other pathogens including viruses and bacteria.

EXPERIMENTAL PROCEDURES

Cells, Mice, and Parasites

C57BL/6 mice were obtained from SLC. ME49 and CTG derivatives of *T. gondii* were maintained in Vero cells by biweekly passage in RPMI1640 (Nacalai Tesque) supplemented with 2% heat-inactivated fetal calf serum (JRH Bioscience), 100 U/ml penicillin, and 0.1 mg/ml streptomycin (GIBCO). MyD88-deficient mice were kindly provided by S. Akira. Animal experiments were conducted with the approval of the Animal Research Committee of the Graduate School of Medicine and of the Research Institute for Microbial Diseases, Osaka University.

Reagents

Antibodies against *T. gondii* (sc-73210), TGTP (Irgb6; sc-11079), Atg4b (sc-130968), Gbp1 (sc-10586), Gbp2 (sc-10588), Gbp5 (sc-160356), Gbp1-5 (sc-166960), and actin (sc-8432) were purchased from Santa Cruz. Anti-CD11b (M1/70) was obtained from Becton Dickinson. Aminoguanidine hydrochloride, LPS (a TLR4 ligand) from *Salmonella minnesota* Re 595, and anti-Flag were purchased from Sigma. Anti-GAP45 rabbit and anti-MIC2 mouse antibodies were as described previously (Frénal et al., 2010). Anti-Irga6 (165/3) and Irgb10 (940/6) rabbit antibodies and anti-Irgm3 (BD Transduction Laboratories) mouse antibodies were kindly provided by J. Howard. Anti-IFN-γ (BE0055) and control Rat IgG1 (BE0088) were obtained from BioXcell. Recombinant IFN-γ and TNF-α were obtained from Peprotech.

In Vivo Measurement of Parasites by Imaging

Mice were intraperitoneally infected with 1×10^2 freshly egressed ME49 tachyzoites expressing luciferase resuspended in 100 μl PBS, and bioluminescence was assessed on the indicated days after infection. Treatment of anti-IFN-γ and control IgG was performed by the intraperitoneal injection 1 day before *T. gondii* infection. For the detection of bioluminescence emission, mice were intraperitoneally injected with 3 mg of D-luciferin in 200 μl PBS (Promega), maintained for 5 min to allow adequate dissemination of the luciferin, then anesthetized with isoflurane (Dainippon Sumitomo Pharma). At 10 min postinjection of D-luciferin, abdominal photon emission was assessed during a 60 s exposure by an in vivo imaging system (IVIS 100; Xenogen) and analyzed as described previously (Yamamoto et al., 2011).

Immunofluorescence

Peritoneal macrophages (1×10^6) infected with *T. gondii* (moi = 0.5) were fixed for 10 min in PBS containing 3.7% formaldehyde. Cells were permeabilized with PBS containing 0.1% Triton X-100 and then blocked with 8% fetal calf serum in PBS. Subsequently, cells were incubated with anti-CD11b rat antibody (1:200) and anti-GAP45 rabbit antibody (1:1,000) in Figure 3D; anti-Atg4b rabbit antibody (1:200) and anti-*T. gondii* mouse antibody (1:50) in Figure 4B; anti-GAP45 rabbit antibody (1:1,000), anti-Irgb6 goat antibody (1:50), and anti-Gbp1-5 mouse antibody (1:200) in Figure 6; and anti-Irgb10 or anti-Irga6 rabbit antibody (1:1,000) and anti-MIC2 mouse antibody (1:1,000), anti-Irgm3 mouse antibody (1:250), and anti-GAP45 rabbit antibody (1:1,000) in Figure S5, for 1 hr at 37°C, followed by incubation with donkey IgG antibodies (1:10,000): Alexa Fluor 488-conjugated anti-rabbit IgG, Alexa Fluor 594-conjugated anti-goat, or Alexa Fluor 647 or Alexa Fluor 594-conjugated anti-mouse (Molecular Probes) for 1 hr at room temperature in the dark. Finally, the immunostained cells were mounted with PermaFluor (Thermo Scientific) on glass slides and analyzed by confocal laser microscopy (FV1000-D IX-81; Olympus); the images were analyzed with Fluoview (Olympus).

Transmission Electron Microscopy

Peritoneal macrophages (1×10^6) untreated or treated with 100 ng/ml IFN-γ for 24 hr were infected with *T. gondii* (moi = 0.5) for 6 or 24 hr. After washing with PBS, the cells were fixed with 2.5% glutaraldehyde in 0.1 M phosphate buffer at 4°C overnight. The cells were postfixed with 1% OsO_4 in the same buffer at 4°C for 1 hr, dehydrated in a graded series of ethanol, and embedded in Quetol 812 (Nissin EM). Silver sections were cut with an ultramicrotome, stained with lead citrate and uranyl acetate, and observed with an H-7650 electron microscope (Hitachi).

Statistical Analysis

The unpaired Student's t test was used to determine the statistical significance of the experimental data.

SUPPLEMENTAL INFORMATION

Supplemental Information includes Supplemental Experimental Procedures, five figures, and one table and can be found with this article online at http://dx.doi.org/10.1016/j.immuni.2012.06.009.

ACKNOWLEDGMENTS

We thank C. Hidaka for excellent secretarial assistance, Y. Magota and M. Enomoto for technical assistance, and members of K.T.'s lab for discussions. Rabbit anti-Irgb6 and Irgb10 and mouse anti-Irgm3 were kindly provided by J.C. Howard. This work was supported by grants from the Ministry of Education, Culture, Sports, Science and Technology; Kanae Foundation for the Promotion of Medical Science; The Cell Science Research Foundation; Kato Memorial Bioscience Foundation; The Uehara Memorial Foundation; Naito Foundation; Mochida Memorial Foundation for Medical and Pharmaceutical Research; The Waksman Foundation of Japan Inc.; Senri Life Science Foundation; The Tokyo Biochemical Research Foundation; The Research Foundation for Microbial Diseases of Osaka University; The Nakajima Foundation; The Asahi Glass Foundation; and The Osaka Foundation for Promotion of Clinical Immunology. M.Y. and D.S.-F. are supported by the Japanese-Swiss bilateral program of The Strategic International Cooperative Program (Research Exchange Type), the Japan Science and Technology Agency (JST).

Received: February 8, 2012
Revised: April 23, 2012
Accepted: June 11, 2012
Published online: July 12, 2012

REFERENCES

Adams, L.B., Hibbs, J.B., Jr., Taintor, R.R., and Krahenbuhl, J.L. (1990). Microbiostatic effect of murine-activated macrophages for *Toxoplasma gondii*. Role for synthesis of inorganic nitrogen oxides from L-arginine. J. Immunol. *144*, 2725–2729.

Aliberti, J., Valenzuela, J.G., Carruthers, V.B., Hieny, S., Andersen, J., Charest, H., Reis e Sousa, C., Fairlamb, A., Ribeiro, J.M., and Sher, A. (2003). Molecular mimicry of a CCR5 binding-domain in the microbial activation of dendritic cells. Nat. Immunol. *4*, 485–490.

Boehm, U., Klamp, T., Groot, M., and Howard, J.C. (1997). Cellular responses to interferon-gamma. Annu. Rev. Immunol. *15*, 749–795.

Boothroyd, J.C. (2009). *Toxoplasma gondii*: 25 years and 25 major advances for the field. Int. J. Parasitol. *39*, 935–946.

Boothroyd, J.C., and Dubremetz, J.F. (2008). Kiss and spit: the dual roles of *Toxoplasma rhoptries*. Nat. Rev. Microbiol. *6*, 79–88.

Collazo, C.M., Yap, G.S., Sempowski, G.D., Lusby, K.C., Tessarollo, L., Woude, G.F., Sher, A., and Taylor, G.A. (2001). Inactivation of LRG-47 and IRG-47 reveals a family of interferon gamma-inducible genes with essential, pathogen-specific roles in resistance to infection. J. Exp. Med. *194*, 181–188.

Collazo, C.M., Yap, G.S., Hieny, S., Caspar, P., Feng, C.G., Taylor, G.A., and Sher, A. (2002). The function of gamma interferon-inducible GTP-binding protein IGTP in host resistance to *Toxoplasma gondii* is Stat1 dependent and requires expression in both hematopoietic and nonhematopoietic cellular compartments. Infect. Immun. *70*, 6933–6939.

Copeland, N.G., Jenkins, N.A., and Court, D.L. (2001). Recombineering: a powerful new tool for mouse functional genomics. Nat. Rev. Genet. *2*, 769–779.

Degrandi, D., Konermann, C., Beuter-Gunia, C., Kresse, A., Würthner, J., Kurig, S., Beer, S., and Pfeffer, K. (2007). Extensive characterization of IFN-induced GTPases mGBP1 to mGBP10 involved in host defense. J. Immunol. *179*, 7729–7740.

Deretic, V. (2006). Autophagy as an immune defense mechanism. Curr. Opin. Immunol. *18*, 375–382.

Fentress, S.J., Behnke, M.S., Dunay, I.R., Mashayekhi, M., Rommereim, L.M., Fox, B.A., Bzik, D.J., Taylor, G.A., Turk, B.E., Lichti, C.F., et al. (2010). Phosphorylation of immunity-related GTPases by a *Toxoplasma gondii*-secreted kinase promotes macrophage survival and virulence. Cell Host Microbe *8*, 484–495.

Frénal, K., Polonais, V., Marq, J.B., Stratmann, R., Limenitakis, J., and Soldati-Favre, D. (2010). Functional dissection of the apicomplexan glideosome molecular architecture. Cell Host Microbe *8*, 343–357.

Gorbacheva, V.Y., Lindner, D., Sen, G.C., and Vestal, D.J. (2002). The interferon (IFN)-induced GTPase, mGBP-2. Role in IFN-gamma-induced murine fibroblast proliferation. J. Biol. Chem. *277*, 6080–6087.

Guenzi, E., Töpolt, K., Cornali, E., Lubeseder-Martellato, C., Jörg, A., Matzen, K., Zietz, C., Kremmer, E., Nappi, F., Schwemmle, M., et al. (2001). The helical domain of GBP-1 mediates the inhibition of endothelial cell proliferation by inflammatory cytokines. EMBO J. *20*, 5568–5577.

Guenzi, E., Töpolt, K., Lubeseder-Martellato, C., Jörg, A., Naschberger, E., Benelli, R., Albini, A., and Stürzl, M. (2003). The guanylate binding protein-1 GTPase controls the invasive and angiogenic capability of endothelial cells through inhibition of MMP-1 expression. EMBO J. *22*, 3772–3782.

Howard, J.C., Hunn, J.P., and Steinfeldt, T. (2011). The IRG protein-based resistance mechanism in mice and its relation to virulence in *Toxoplasma gondii*. Curr. Opin. Microbiol. *14*, 414–421.